PERGAMON International Journal of Non-Linear Mechanics 37 (2002) 801–831

INTERNATIONAL JOURNAL OF NON-LINEAR MECHANICS

www.elsevier.com/locate/ijnonlinmec

Global optimum design of externally pressurized isogrid stiffened cylindrical shells with added T-rings

David Bushnell

Department L9-24, Building 204, Lockheed Martin Advanced Technology Center, 3251 Hanover St., Palo Alto, CA 94304-1911, USA

Abstract

PANDA2 is a code for the minimum-weight design of perfect and imperfect elastic stiffened panels and shells made of composite laminates and subjected to multiple sets of in-plane loads, edge moments, normal pressure, and temperature. The scope of PANDA2 is increased to include global optimization and the capability to handle isogrid stiffening. The enhanced program is used to find global optimum designs of internally T-isogrid and internally T-ring stiffened perfect and imperfect isotropic cylindrical shells under uniform external pressure. For the cases studied, it is found that for the perfect optimized shells the isogrid stiffening is important but the rings are not, whereas the opposite holds for the optimized shells with an initial general buckling modal imperfection of amplitude equal to one per cent of the shell radius © 2002 Published by Elsevier Science Ltd.

1. Introduction

This paper reports the use of the structural optimization code, PANDA2, to find minimum-weight designs of perfect and imperfect internally T-isogrid stiffened cylindrical shells with internal rings with T-shaped cross sections. An isogrid stiffened skin has three sets of identical stiffeners that divide the skin into equilateral triangles [1]. In PANDA2 [2–11] there are two possible orientations of the isogrid stiffening pattern; (1) one of the three sets of stiffeners runs in the circumferential direction and (2) one of the three sets of stiffeners runs in the axial direction. In all of the examples presented here Option 1 is used. The three sets of isogrid stiffeners are identified as "isogrd1, isogrd2, isogrd3", with the stiffener axes oriented at +30 degrees, −30 degrees, and 90 degrees, respectively, relative to the axial coordinate, which is the generator of the cylindrical shell.

1.1. Statement of the problem

All of the examples here pertain to a complete (360-degree) simply supported cylindrical shell of length 35 in and radius to the skin middle surface of 9.4 in. The stiffeners are internal. All stiffeners have T-shaped cross sections. The cross section dimensions of the isogrid members are different from those of the rings. The material is titanium and remains elastic. The cylindrical shell is loaded by uniform external pressure of 1500 psi. The optimization problem is completely set forth in Table 1. Optimum designs for several cases are

E-mail address: bush@trinity.atc.imco.com (D. Bushnell).

0020-7462/02/$ - see front matter © 2002 Published by Elsevier Science Ltd.
PII: S0020-7462(01)00100-7

Table 1
Internally isogrid stiffened cylindrical shell with internal T-rings

Parameters from which decision variables can be chosen in "decide"

Variable no.	Name	Starting value (in)	Definition	Decision variable?
1	B(ISO) =	1.000:	stiffener spacing, b (isogrid stiffeners)	yes
2	B2(ISO) =	0.333:	width of isogrid base, b2 (no input needed) (Seg. 2)	no
3	H(ISO) =	0.500:	height of stiffener, h (isogrid stiffeners; (Seg. 3)	yes
4	W(ISO) =	0.200:	width of outstanding flange of isogrid, w (Seg. 4)	yes
5	T1(SKN) =	0.100:	thickness for layer index no. (1), panel skin (Seg. 1)	yes
6	T2(ISO) =	0.050:	thickness for layer index no. (2), isogrid web	yes
7	T3(ISO) =	0.050:	thickness for layer index no. (3), isogrid flange	yes
8	B(RNG) =	10.000:	stiffener spacing, b (ring stiffeners)	yes
9	B2(RNG) =	0.000:	width of ring base, b2 (Seg. 2)	no
10	H(RNG) =	1.000:	height of stiffener, h (ring stiffeners; Seg. 3)	yes
11	W(RNG) =	1.000:	width of outstanding flange of ring, w (Seg. 4)	yes
12	T4(RNG) =	0.100:	thickness for layer index no. (4), ring web	yes
13	T5(RNG) =	0.100:	thickness for layer index no. (5), ring flange	yes

Parameters which are always fixed, none can be decision variables:

Value (in)	Definition	
3.500E + 01	Panel length normal to the plane of the screen, L1 (axial length)	
2.953E + 01	Panel length in the plane of the screen, L2 (length = pi x radius)	
G	Type of stiffener along L1 (N, T, J, R, A, C, G) (G = isogrid)	
T-Shaped	Type of isogrid stiffener cross section (T, J, R)	
0.1640E + 08	Young's modulus (psi), E	(Note: In the input data listed
0.3100	Poisson's ratio, NU	in Table 9 of [7] there are two
6260000.	Transverse shear modulus G13	materials: 1 for skin and isogrid
0	Thermal expansion coeff., ALPHA	and 2 for rings. 1 and 2 are same.
0	Residual stress temp., TEMPTUR	Purpose is to smooth the evolution
108000.	Max allowable effective stress.	of the design and to show stress
0.1600	Matl weight density (lbs/in^3)	margins for both skin/isogrid & for rings.)
1	Choose orientation (1 or 2) of isogrid. (1 = member no. 3 is circumferential.)	
1	Choose external (0) or internal (1) isogrid stiffeners	
T-SHAPED	Identify type of stiffener along L2 (N, T, J, Z, R, A) (rings)	
1	Choose external (0) or internal (1) rings:	
9.400E + 00	Radius of curvature in the plane of screen, R (cylindrical shell)	
0	Prebuckling phase (0 = simple support or 1 = clamping or Z = infinite)	
0	Buckling phase (0 = simple support or 1 = clamping)	
1500	Uniform external pressure, p; Resultants $N_x = -pR/2$; $N_y = -pR$, $N_{xy} = 0$	

User-provided factors of safety (FS):
1.33 = FS for general buckling; 1.10 = FS for inter-ring buckling;
1.00 = FS for stiffener buckling; 1.00 = FS for stress.
(Other FS in Table 3 are computed or assigned by PANDA2.)

Equality and inequality constraints provided as input in "decide":
equality constraint: $B2(ISO) = 0.100 \times B(ISO)$
inequality constraints: $2.0 > H(RNG) + T1(SKN) + 0.5 \times T5(RNG)$
$B(RNG) > 3.0 \times B(ISO)$

Lower and upper bounds of decision variables chosen in "decide":
$(0.4 < B(ISO) < 3.0)$, $(0.05 < H(ISO) < 1.0)$, $(0.02 < W(ISO) < 0.5)$, $(0.02 < T1(SKN) < 10.)$
$(0.02 < T2(ISO) < 10.)$, $(0.02 < T3(ISO) < 10.)$, $(5.0 < B(RNG) < 20.)$, $(0.5 < H(RNG) < 3.0)$
$(0.1 < W(RNG) < 4.0)$, $(0.02 < T4(RNG) < 10.)$, $(0.02 < T5(RNG) < 10.)$,
Note: The lower bound of B(ISO) is raised to 2.0 for the cases in Columns 8, 9, and 12 of Tables 2 and 4 (perfect and imperfect shells without rings).

listed in Table 2. Design margin definitions are listed in Table 3, and design margin values for several optimum designs are listed in Tables 4 and 5. The imperfect shells have an initial imperfection in the form of the general buckling mode with amplitude, $W_{\text{imp}} = 0.094$ in. There are no additional inter-ring or local panel skin buckling modal imperfections.

In PANDA2 a complete (360-degree) cylindrical shell is modelled as a panel that spans 180 degrees [2,6,10]. Boundary conditions on all four edges of this panel are classical simple support (antisymmetry) for buckling. The overall buckling behavior of a 180-degree panel simply supported along its two generators is identical to that of a complete (360-degree) cylindrical shell [2]. The optimum weights listed in Table 2, therefore, represent half (180 degrees) of the cylindrical shell.

2. Brief description of PANDA2

PANDA2 is a computer program for the minimum weight design of stiffened, composite, flat or cylindrical, perfect or imperfect panels and shells subjected to multiple sets of combined in-plane loads, normal pressure, edge moments, and temperature. For most configurations, the panels can be locally postbuckled [4]. Local postbuckling of the panel skin between isogrid stiffeners is not permitted, however. Previous work on PANDA2 is documented in [2–11]. PANDA2 incorporates the theories of earlier codes PANDA [3] and BOSOR4 [12–16]. The optimizer used in PANDA2 is called ADS [17].

Global optimum designs can be obtained with PANDA2 by means of a processor called "SUPEROPT", which is described in more detail in [7]. At intervals during the optimization process new "starting" designs are automatically generated as follows:

$$y(i) = x(i)[1 + \mathrm{d}x(i)],$$

$$i = 1, 2, 3 \ldots \text{number of decision variables} \qquad (1)$$

in which $x(i)$ is the old value of the $i$the decision variable, $y(i)$ is the new value, and $\mathrm{d}x(i)$ is a random number between -0.5 and $+1.5$ if the decision variable is other than a stiffener spacing and a random number between -1.0 and $+1.0$ if the decision variable is a stiffener spacing. The difference in treatment for decision variables that are not stiffener spacings from those that are results from early experiments with SUPEROPT [7].

2.1. Types of buckling included in PANDA2

As described in [2,3,10], PANDA2 computes general, inter-ring, and local skin buckling loads and mode shapes. General buckling is buckling in which both stringers (or isogrid stiffeners) and rings participate; "panel" (inter-ring) buckling is buckling between adjacent rings in which stringers (or isogrid stiffeners) participate but the lines of intersection of ring web roots with the panel skin do not translate; local buckling is buckling of the panel skin between adjacent stringers (or isogrid stiffeners) and rings.

Over the years an elaborate strategy has been developed in order to ensure that for each type of buckling the most critical (lowest) buckling load factor has not been missed. An example involving general buckling of the shell listed in Column 10 of Table 2 is given in Part 4 of Table 6. There are six values listed in the row entitled "EIGGEN". These values are derived from searches over various regions in the (m, n, slope) domain, where m is the number of axial halfwaves, n is the number of circumferential halfwaves, and "slope" is the slope of the buckling nodal lines (non-zero when there is in-plane shear loading and/or shell wall anisotropy). The first value of EIGGEN results from a search over the (low-m, low-n) region; the second from a search over the (low-m, low-n) region; the third from a search over the (high-m, low-n) region; the fourth from a search over the (high-m, low-n) region; the fifth from a search over a wide range of (m, n) with "slope"$= 0$; and the sixth from a search over several (m, n) pairs missed by the previous searches. There is also a seventh search, not shown in Table 6, for possible axisymmetric buckling, $(m, 0)$.

PANDA2 also computes buckling load factors for several different kinds of local buckling and rolling of stiffener segments (web and outstanding

Table 2
Optimized designs of internally isogrid-stiffened cylindrical shells with internal T-shaped rings. Dimensions are in inches[a]

Variable name	Columns 1–9 pertain to perfect optimized shells Columns 1–7 with stress constraint; Columns 8, 9 no stress constraint									Columns 10–12 for imperfect shells Wimp = 0.094 in; yes stress constraint		
	Column 1	Column 2	Column 3	Column 4	Column 5	Column 6	Column 7	Column 8	Column 9	Column 10	Column 11[b]	Column 12
B(ISO)	1.91E + 00	1.67E + 00	2.46E + 00	2.56E + 00	2.39E + 00	2.22E + 00	2.00E + 00	8.44E − 01	2.13E + 00	1.91E + 00	1.66E + 00	3.00E + 00
B2(ISO)	1.91E − 01	1.67E − 01	2.46E − 01	2.56E − 01	2.39E − 01	2.22E − 01	2.00E − 01	8.44E − 02	2.13E − 01	1.91E − 01	1.66E − 01	3.00E − 01
H(ISO)	6.24E − 01	5.54E − 01	6.71E − 01	6.90E − 01	7.37E − 01	8.18E − 01	8.90E − 01	2.89E − 01	8.83E − 01	6.24E − 01	6.79E − 01	9.87E − 01
W(ISO)	3.17E − 01	3.12E − 01	3.38E − 01	3.56E − 01	3.41E − 01	3.32E − 01	3.12E − 01	1.95E − 01	3.26E − 01	3.17E − 01	4.48E − 01	4.06E − 01
T1(SKN)	9.28E − 02	9.25E − 02	1.03E − 01	1.06E − 01	9.96E − 02	9.34E − 02	8.88E − 02	4.95E − 02	8.93E − 02	9.28E − 02	1.08E − 01	1.67E − 01
T2(ISO)	2.65E − 02	2.35E − 02	2.89E − 02	2.96E − 02	3.17E − 02	3.62E − 02	3.80E − 02	2.00E − 02	3.76E − 02	2.65E − 02	2.58E − 02	4.02E − 02
T3(ISO)	3.22E − 02	2.89E − 02	3.72E − 02	3.57E − 02	3.85E − 02	4.18E − 02	4.69E − 02	2.53E − 02	4.69E − 02	3.22E − 02	3.64E − 02	1.31E − 01
B(RNG)	5.74E + 00	5.00E + 00	8.75E + 00	11.67E + 00	17.50E + 00	35.00E + 00	—	5.00E + 00	—	5.74E + 00	5.00E + 00	—
B2(RNG)	0.00E + 00	0.00E + 00	0.00E + 00	0.00E + 00	0.00E + 00	0.00E + 00	—	0.00E + 00	—	0.00E + 00	0.00E + 00	—
H(RNG)	1.21E + 00	1.22E + 00	1.31E + 00	1.40E + 00	1.48E + 00	1.45E + 00	—	1.52E + 00	—	1.21E + 00	1.53E + 00	—
W(RNG)	5.37E − 01	5.03E − 01	5.49E − 01	6.00E − 01	5.81E − 01	5.23E − 01	—	9.94E − 01	—	5.37E − 01	6.54E − 01	—
T4(RNG)	6.23E − 02	6.41E − 02	6.72E − 02	6.79E − 02	7.65E − 02	7.93E − 02	—	8.06E − 02	—	6.23E − 02	1.08E − 01	—
T5(RNG)	5.39E − 02	4.70E − 02	4.07E − 02	4.37E − 02	4.36E − 02	6.98E − 02	—	4.61E − 02	—	5.39E − 02	1.83E − 01	—
Weight (lbs)[c]	25.29	25.21	25.55	25.63	25.37	25.88	26.69	20.03	26.09	25.29	37.36	43.01

[a] *Note*: The definitions corresponding to the variable names in the leftmost column are listed in Table 1. Column 1: perfect shell, ring spacing is decision variable; Column 2: perfect shell, ring spacing fixed at 5 in; Column 3: perfect shell, ring spacing fixed at 8.75 in; Column 4: perfect shell, ring spacing fixed at 11.6667 in; Column 5: perfect shell, ring spacing fixed at 17.5 in; Column 6: perfect shell, ring spacing fixed at 35.00 in; Column 7: perfect shell, no rings (lwr bound of B(ISO) = 2.0); Column 8: perfect shell optimized with maximum allowable stress increased by a factor of 10; Column 9: perfect shell, no rings, stress constraint as ln 8; Column 10: imperfect shell, same design as that for Column 1; Wimp = 0.094 in; Column 11: imperfect shell, ring spacing is decision variable; Column 12: imperfect shell, optimized with no rings (lower bound of B(ISO) = 2.0).

[b] *Note*: Column 11 dimensions above were obtained after the 1st execution of SUPEROPT. During the 2nd SUPEROPT the isogrid stiffeners almost disappeared: Imperfect shell (new Column 11 dimensions after 2nd SUPEROPT): B(ISO) = 1.67; B2(ISO) = 0.167; H(ISO) = 0.116; W(ISO) = 0.348; T1(SKN) = 0.164; T2(ISO) = 0.020; T3(ISO) = 0.020; B(RNG) = 5.0; H(RNG) = 1.41; W(RNG) = 0.718; T4(RNG) = 0.0875; T5(RNG) = 0.121; WEIGHT = 36.85 lbs. This design is not practical, but indicates that optimization should be performed without isogrid. Next two lines, optimized perfect and imperfect shells with rings but no isogrid (dimensions in inches): Perfect shell with rings but no isogrid: T1(SKN) = 0.190; B(RNG) = 5.00; H(RNG) = 1.19; W(RNG) = 0.588; T4(RNG) = 0.0423; T5(RNG) = 0.0365; WEIGHT = 33.80 lbs Imperf. shell with rings but no isogrid: T1(SKN) = 0.196; B(RNG) = 5.00; H(RNG) = 1.27; W(RNG) = 0.576; T4(RNG) = 0.0846; T5(RNG) = 0.1235; WEIGHT = 38.30 lbs.

[c] WEIGHT is the weight in lbs of half (180 degrees) of the complete stiffened cylindrical shell.

Table 3
Definitions of design margins for isogrid stiffened cylindrical shell with added T-rings

Margins for subcase no. 1 (conditions midway between rings)	
Margin number	Definition
1	Inter-ring buckling, discrete model, $n=6$ circ.halfwaves; FS = 1.1
2	Ring sidesway backl., discrete model, $n=4$ circ.halfwaves; FS = 1.1
3	Hi-n Ring web buckl., discrete model, $n=21$ circ.halfwaves; FS = 1.1
4	Lo-n Ring sidesway, discrete model, $n=2$ circ.halfwaves; FS = 1.1
5	eff.stress:matl = 1, SKN, Iseg = 2, at: $n=6$, layer = 1, $z=0.0247$; -MID.; FS = 1.
6	eff.stress:matl = 1, ISO, Iseg = 4, allnode, layer = 1, $z=-0.0161$; -MID.; FS = 1.
7	eff.stress:matl = 2, RNG, Iseg = 4, allnode, layer = 1, $z=-0.0302$; -MID.; FS = 1.
8	buckling margin isogrd1 web. Local halfwaves = 3 .MID.; FS = 1.
9	buckling margin isogrd2 web. Local halfwaves = 3 .MID.; FS = 1.
10	buckling margin isogrd3 web. Local halfwaves = 2 .MID.; FS = 1.
11	buckling margin isogrd3 flange. Local halfwaves = 2 .MID.; FS = 1.
12	buckling isogrd3 Isegs. 3 + 4 together. $M=3$; $C=0$; MID.; FS = 1.4.
13	buckling isogrd3 stiff. no. j = 3; panel MID.; $M=1$; FS = 1.2.
14	buckling margin ring Iseg.3 Local halfwaves = 21 .MID.; FS = 1.
15	buckling ring Iseg 4 as beam on foundation. $M=2$; MID.; FS = 3.
16	buck. (SAND); simp-support inter-ring buck; $M=1$; $N=6$; slope = 0.; FS = 1.1.
17	buck. (SAND); simp-support general buck; $M=1$; $N=2$; slope = 0.; FS = 3333.
18	buck. (SAND); rolling only of isogrid3; $M=1$; $N=0$; slope = 0.; FS = 1.6.
19	buck. (SAND); hiwave roll. of isogrid3; $M=3$; $N=0$; slope = 0.; FS = 1.2.
20	buck. (SAND); rolling only axisym. rings; $M=0$; $N=0$; slope = 0.; FS = 1.6.
21	buck. (SAND); ISOGRID : web buckling; $M=3$; $N=1$; slope = 0.; FS = 1.
22	buck. (SAND); RINGS : web buckling; $M=15$; $N=1$; slope = 0.; FS = 1.
23	Local triangular skin buckling load factor −1; FS = 1.1.
24	(Max. allowable ave. axial strain)/(ave.axial strain) −1; FS = 1.
25	0.3333*(Stringer spacing, b)/(Stringer base width, b2) −; FS = 1.
26	1 − [0. + 0.5V(10)⌉ + 0.5V(5)⌉ + 0.25V(13)⌉]
27	1 − [1. + 3.V(1)⌉ − V(8)⌉]

Margins for subcase no. 2 (conditions at the ring stations)	
Margin number	Definition
1	Inter-ring buckling, discrete model, $n=6$ circ.halfwaves; FS = 1.1.
2	Ring sidesway buckl., discrete model, $n=4$ circ.halfwaves; FS = 1.1.
3	Hi-n Ring web buckl., discrete model, $n=21$ circ.halfwaves; FS = 1.1.
4	Hi-n Ring sidesway ,discrete model, $n=48$ circ.halfwaves; FS = 1.1.
5	Lo-n Ring sidesway, discrete model, $n=2$ circ.halfwaves; FS = 1.1.
6	eff.stress:matl = 1, SKN, Iseg = 2, at: $n=6$, layer = 1, $z=0.0247$; -RNGS; FS = 1.
7	eff.stress:matl = 1, ISO, Iseg = 4, allnode, layer = 1, $z=-0.0161$; -RNGS; FS = 1.
8	eff.stress:matl = 2, RNG, Iseg = 4, allnode, layer = 1, $z=-0.0302$; -RNGS; FS = 1.
9	buckling margin isogrd1 web. Local halfwaves = 3 .RNGS; FS = 1.
10	buckling margin isogrd2 web. Local halfwaves = 3 .RNGS; FS = 1.
11	buckling margin isogrd3 web. Local halfwaves = 2 .RNGS; FS = 1.
12	buckling margin isogrd2 flange. Local halfwaves = 2 .RNGS; FS = 1.
13	buckling isogrd2 Isegs. 3 + 4 together. $M=3$; $C=0$; RNGS; FS = 1.4.
14	buckling isogrd2 stiff. no. j = 2; panel RNGS;$M=1$; FS = 1.2.
15	buckling margin ring Iseg 3. Local halfwaves = 21 .RNGS; FS = 1.
16	buckling margin ring Iseg 4. Local halfwaves = 21 .RNGS; FS = 1.
17	buckling ring Isegs 3 + 4 together. $M=26$; $C=0.$; .RNGS; FS = 1.
18	buckling ring Isegs 4 as beam on foundation. $M=2$; RNGS;FS = 3.
19	buck. (SAND); rolling only of isogrid2; $M=1$; $N=0$; slope = 0.; FS = 1.6.
20	buck. (SAND); hiwave roll. of isogrid2; $M=3$; $N=0$; slope = 0.; FS = 1.2.
21	buck. (SAND); rolling only of rings; $M=0$; $N=3$; slope = 0.; FS = 1.6.
22	buck. (SAND); hiwave roll. of rings; $M=0$; $N=28$; slope = 0.; FS = 1.365.
23	buck. (SAND); rolling only axisym.rings; $M=0$; $N=0$; slope = 0.; FS = 1.6
24	buck. (SAND); ISOGRID : web buckling; $M=3$; $N=1$; slope = 0.; FS = 1.
25	buck. (SAND); RINGS : web buckling; $M=15$; $N=1$; slope = 0.; FS = 1.
26	Local triangular skin buckling load factor −1; FS = 1.1.

Table 4
Margins corresponding to optimized designs of isogrid-stiffened cylindrical shell with T-shaped rings; Subcase 1: midway between ring[a]

Margin number	Columns 1–9 pertain to perfect optimized shells Columns 1–7 with stress constraint; Columns 8,9 no stress constraint									Columns 10–12 for imperfect shells Wimp = 0.094 in.: yes stress constraint		
	Column 1	Column 2	Column 3	Column 4	Column 5	Column 6	Column 7	Column 8	Column 9	Column 10	Column 11	Column 12
1	-,—	-,—	-,—	-,—	-,—	−4.37E − 02	6.66E − 02	−1.83E − 03	2.00E − 02	-,—	-,—	1.20E + 00
2	4.29E − 03	−1.79E − 02	7.92E − 02	−1.02E − 02	−4.43E − 03	-,—	-,—	-,—	-,—	−7.61E − 01	6.94E − 03	-,—
3	6.82E − 01	7.06E − 01	6.46E − 01	5.28E − 01	6.99E − 01	-,—	-,—	−4.83E − 02	-,—	−7.48E − 01	3.01E + 00	-,—
4	-,—	-,—	-,—	-,—	-,—	-,—	-,—	−1.58E − 02	-,—	-,—	-,—	-,—
5	−1.83E − 03	6.87E − 03	9.46E − 03	2.50E − 02	9.87E − 03	−3.99E − 05	−4.29E − 06	4.47E + 00	8.92E + 00	-,—	1.56E − 01	-,—
6	-,—	-,—	-,—	-,—	-,—	-,—	-,—	-,—	-,—	−8.37E − 01	-,—	−4.95E − 02
7	8.80E − 04	−2.07E − 03	−2.00E − 05	4.59E − 05	1.49E − 03	1.76E − 01	-,—	4.43E + 00	-,—	−9.05E − 01	−3.61E − 03	-,—
8	1.98E + 00	1.93E + 00	1.96E + 00	1.61E + 00	1.47E + 00	1.48E + 00	1.49E + 00	5.12E + 00	1.55E + 00	−3.65E − 01	1.64E + 01	1.33E + 00
9	1.85E + 00	1.80E + 00	1.83E + 00	1.52E + 00	1.39E + 00	1.39E + 00	1.41E + 00	4.78E + 00	1.47E + 00	−3.71E − 01	1.52E + 01	1.27E + 00
10	1.68E − 02	1.23E − 02	1.28E − 03	7.76E − 04	4.85E − 02	4.08E − 02	4.68E − 02	5.09E − 01	7.27E − 02	−7.38E − 01	4.63E − 03	−2.81E − 02
11	1.67E + 00	1.34E + 00	2.13E + 00	1.64E + 00	2.09E + 00	2.78E + 00	4.01E + 00	1.64E + 00	3.59E + 00	−5.88E − 01	9.60E − 01	1.50E + 01
12	3.13E − 03	5.78E − 03	7.62E − 02	−9.30E − 04	1.52E − 02	4.06E − 03	−5.91E − 04	4.18E − 01	−7.55E − 03	−7.71E − 01	8.22E − 02	4.24E + 00
13	3.57E − 01	5.01E − 01	−6.29E − 03	9.06E − 03	−1.77E − 03	−1.29E − 03	9.62E − 05	6.56E − 01	−2.17E − 01	−7.66E − 01	5.00E − 01	7.10E − 02
14	4.17E − 01	5.05E − 01	5.64E − 01	4.31E − 01	6.08E − 01	7.36E − 01	-,—-	3.31E − 01	-,—-	−7.71E − 01	2.35E + 00	-,—-
15	1.42E + 00	1.36E + 00	1.25E + 00	1.30E + 00	1.34E + 00	2.12E + 00	-,—-	6.90E − 01	-,—-	−8.02E − 01	2.63E + 00	-,—-
16	-,—-	-,—-	-,—-	-,—-	-,—-	-,—-	-,—-	-,—-	-,—-	-,—-	-,—-	-,—-
17	−7.60E − 03	−1.34E − 02	−1.10E − 02	−6.89E − 03	−1.95E − 02	−9.24E − 03	−3.56E − 03	−1.86E − 02	−4.86E − 02	−1.36E − 01	1.10E + 00	9.04E − 01
18	3.70E − 01	9.37E − 01	3.26E − 02	5.05E − 02	3.71E − 02	4.46E − 02	4.80E − 02	5.83E − 01	4.03E − 02	−7.54E − 01	8.15E − 01	4.07E − 02
19	1.05E + 00	-,—-	1.27E + 00	1.02E + 00	1.18E + 00	1.28E + 00	1.15E + 00	1.31E + 00	1.15E + 00	−6.10E − 01	-,—-	-,—-
20	−4.01E − 02	3.64E − 02	9.92E − 02	−2.56E − 03	6.71E − 02	2.04E − 02	-,—-	5.89E − 02	-,—-	−9.01E − 01	1.41E − 02	-,—-
21	3.47E − 03	1.02E − 02	2.77E − 04	−2.32E − 04	3.55E − 03	3.98E − 02	−1.37E − 04	5.07E − 01	−2.98E − 02	−5.24E − 01	2.92E − 03	2.01E − 01
22	4.10E − 01	4.98E − 01	5.56E − 01	4.24E − 01	5.99E − 01	7.24E − 01	-,—-	3.22E − 01	-,—-	−7.65E − 01	7.76E + 00	-,—-
23	2.72E − 01	6.53E − 01	−1.41E − 02	−1.56E − 02	−1.14E − 02	−8.82E − 03	1.02E − 01	−6.27E − 03	−1.88E − 02	−5.40E − 01	1.44E + 00	1.56E + 00
24	5.26E + 02	5.07E + 02	6.66E + 02	7.39E + 02	7.27E + 02	7.03E + 02	7.07E + 02	2.35E + 02	7.01E + 02	5.26E + 02	5.05E + 02	1.23E + 03
25	2.33E + 00	2.33E + 00	2.33E + 00	2.33E + 00	2.33E + 00	2.33E + 00	2.33E + 00	2.33E + 00	2.33E + 00	2.33E + 00	2.33E + 00	2.33E + 00
26	3.34E − 01	3.34E − 01	2.84E − 01	2.36E − 01	2.02E − 01	2.10E − 01	-,—-	2.05E − 01	-,—-	3.34E − 01	1.37E − 01	-,—-
27	9.97E − 05	1.35E − 04	1.36E + 00	3.98E + 00	1.03E + 01	2.83E + 01	-,—-	2.47E + 00	-,—-	9.97E − 05	3.19E − 02	-,—-

[a] *Note*: The margin definitions corresponding to margin numbers in the leftmost column are listed in the top part of Table 3. Column 1: perfect shell, ring spacing is decision variable; Column 2: perfect shell, ring spacing fixed at 5 in; Column 3: perfect shell, ring spacing fixed at 8.75 in; Column 4: perfect shell, ring spacing fixed at 11.6667 in; Column 5: perfect shell, ring spacing fixed at 17.5 in; Column 6: perfect shell, ring spacing fixed at 35.00 in; Column 7: perfect shell, no rings (lwr bound of B(ISO) = 2.0); Column 8: perfect shell optimized with maximum allowable stress increased by a factor of 10; Column 9: perfect shell, no rings, stress constraint as in 8; Column 10: imperfect shell, same design as that for Col. 1; Wimp = 0.094 in; Column 11: imperfect shell, ring spacing is decision variable; Column 12: imperfect shell, optimized with no rings (lower bound of B(ISO) = 2.0). Next two lines, optimized perfect and imperfect shells with rings but no isogrid. Meaning is "(margin number from top of Table 3)= margin value": Perfect shell with rings but no isogrid: (1) = − 3.11E − 03; (3) = 1.70E − 01; (4) = 1.89E − 02; (14) = 1.65E − 01; (17) = 1.32E − 04; (20) = 5.04E − 03; (22) = 1.61E − 01 Imperf. shell with rings but no isogrid: (1) = − 4.87E − 03; (4) = 1.88E + 00; (7) = − 4.57E − 02; (14) = 2.05E + 00; (17) = 5.16E − 01; (20) = 2.19E − 02; (26) = 2.34E − 01.

Table 5
Margins corresponding to optimized designs of isogrid-stiffened cylindrical shell with T-shaped rings; Subcase 2: at ring station[a]

Margin number	Columns 1–9 pertain to perfect optimized shells Columns 1–7 with stress constraint; Columns 8,9 no stress constraint									Columns 10–12 for imperfect shells Wimp = 0.094 in.; yes stress constraint		
	Column 1	Column 2	Column 3	Column 4	Column 5	Column 6	Column 7	Column 8	Column 9	Column 10	Column 11	Column 12
1	-,—	-,—	-,—	-,—	-,—	−1.97E − 02	-,—	1.13E − 01	-,—	8.57E − 01	-,—	-,—
2	3.30E − 02	6.66E − 03	7.23E − 02	5.53E − 02	4.14E − 02	-,—	-,—	-,—	-,—	-,—	9.78E − 01	-,—
3	7.30E − 01	7.48E − 01	7.51E − 01	6.29E − 01	7.77E − 01	-,—	-,—	6.14E − 02	-,—	-,—	4.92E + 00	-,—
4	-,—	-,—	-,—	-,—	-,—	-,—	-,—	-,—	-,—	2.80E + 00	-,—	-,—
5	-,—	-,—	-,—	-,—	-,—	-,—	-,—	9.77E − 02	-,—	5.11E − 01	-,—	-,—
6	-,—	-,—	-,—	-,—	-,—	-,—	-,—	-,—	-,—	−6.29E − 01	-,—	-,—
7	−1.96E − 04	1.03E − 03	−4.14E − 05	−4.08E − 04	−3.22E − 02	−4.84E − 03	-,—	2.37E + 00	-,—	-,—	−2.49E − 03	-,—
8	8.80E − 04	−2.07E − 03	−2.00E − 05	4.59E − 05	1.49E − 03	1.76E − 01	-,—	4.43E + 00	-,—	−9.05E − 01	−3.61E − 03	-,—
9	3.92E − 01	3.70E − 01	4.29E − 01	4.28E − 01	4.59E − 01	4.99E − 01	-,—	3.40E − 01	-,—	3.33E − 01	1.47E − 01	-,—
10	3.63E − 01	3.41E − 01	4.01E − 01	4.01E − 01	4.31E − 01	4.69E − 01	-,—	3.22E − 01	-,—	3.05E − 01	1.26E − 01	-,—
11	1.24E − 01	1.21E − 01	1.60E − 01	1.59E − 01	1.62E − 01	1.25E − 01	-,—	8.94E − 01	-,—	7.65E − 02	1.07E − 01	-,—
12	1.56E + 00	1.20E + 00	2.04E + 00	1.55E + 00	1.94E + 00	2.73E + 00	-,—	5.00E − 01	-,—	1.56E + 01	6.83E − 01	-,—
13	2.00E − 01	1.60E − 01	3.25E − 01	2.28E − 01	2.52E − 01	3.00E − 01	-,—	2.17E − 03	-,—	2.00E − 01	4.66E − 02	-,—
14	3.92E − 01	6.00E − 01	2.51E − 02	3.63E − 02	1.79E − 02	6.79E − 02	-,—	8.73E − 03	-,—	3.92E − 01	3.77E − 01	-,—
15	4.17E − 01	5.05E − 01	5.64E − 01	4.31E − 01	6.08E − 01	7.36E − 01	-,—	3.31E − 01	-,—	−7.71E − 01	2.35E + 00	-,—
16	-,—	-,—	-,—	-,—	-,—	-,—	-,—	-,—	-,—	−7.58E + 01	1.40E + 01	-,—
17	-,—	-,—	-,—	-,—	-,—	-,—	-,—	-,—	-,—	−8.22E − 01	3.62E + 01	-,—
18	1.42E + 00	1.36E + 00	1.25E + 00	1.30E + 00	1.34E + 00	2.12E + 00	-,—	6.90E − 01	-,—	−8.02E − 01	2.63E + 00	-,—
19	4.39E − 01	7.98E − 01	9.75E − 02	1.13E − 01	9.32E − 02	1.58E − 01	-,—	2.12E − 03	-,—	4.39E − 01	6.34E − 01	-,—
20	1.22E + 00	1.02E + 00	1.52E + 00	1.23E + 00	1.43E + 00	1.72E + 00	-,—	4.70E − 01	-,—	1.22E + 00	-,—	-,—
21	-,—	-,—	-,—	-,—	-,—	-,—	-,—	-,—	-,—	−9.14E − 01	−1.27E − 02	-,—
22	-,—	-,—	-,—	-,—	-,—	-,—	-,—	-,—	-,—	−7.64E − 01	-,—	-,—
23	−4.01E − 02	3.64E − 02	9.92E − 02	−2.56E − 03	6.71E − 02	2.04E − 02	-,—	5.89E − 02	-,—	−9.01E − 01	1.41E − 02	-,—
24	3.54E − 01	3.47E − 01	4.10E − 01	4.10E − 01	3.79E − 01	4.79E − 01	-,—	3.44E − 01	-,—	−9.16E − 01	6.02E − 02	-,—
25	4.10E − 01	4.98E − 01	5.56E − 01	4.24E − 01	5.99E − 01	7.24E − 01	-,—	3.22E − 01	-,—	−7.65E − 01	1.76E + 00	-,—
26	3.47E − 01	7.43E − 01	5.92E − 02	4.80E − 02	2.69E − 02	1.23E − 02	-,—	2.39E − 01	-,—	−5.31E − 01	1.59E + 00	-,—

[a] *Note:* The margin definitions corresponding to the margin numbers in the leftmost column are listed in the bottom part of Table 3. Column 1: perfect shell, ring spacing is decision variable; Column 2: perfect shell, ring spacing fixed at 5 in; Column 3: perfect shell, ring spacing fixed at 8.75 in; Column 4: perfect shell, ring spacing fixed at 11.6667 in; Column 5: perfect shell, ring spacing fixed at 17.5 in; Column 6: perfect shell, ring spacing fixed at 35.00 in; Column 7: perfect shell, no rings (lwr bound of B(ISO) = 2.0); Column 8: perfect shell optimized with maximum allowable stress increased by a factor of 10; Column 9: perfect shell, no rings, stress constraint as in 8; Column 10: imperfect shell, same design as that for Column 1; Wimp = 0.094 in; Column 11: imperfect shell, ring spacing is decision variable; Column 12: imperfect shell, optimized with no rings (lower bound of B(ISO) = 2.0). Next two lines, optimized perfect and imperfect shells with rings but no isogrid. Meaning is "(margin number from bottom of Table 3) = margin value": Perfect shell with rings but no isogrid: (1) = − 3.13E − 03; (3) = 1.69E − 01; (5) = 1.89E − 02; (8) = 4.49E − 01; (15) = 1.65E − 01; (23) = 5.04E − 03; (25) = 1.61E − 01 Imperf.shell with rings but no isogrid: (1) = 7.08E − 02; (5) = 1.80E − 01; (8) = − 4.57E − 02; (15) = 2.05E + 00; (23) = 2.19E − 02; (25) = 1.82E + 00.

Table 6
PANDA2 output that describes effects of initial imperfections and other knockdown factors corresponding to the imperfect cylindrical shell of Column 10 in Table 2

Part 1 Knockdown factors for imperfections derived from PANDA2 theory [6] vs those from ARBOCZ' 1992 update [7,19] of Koiter's 1963 special theory [18]

BUCKLING LOAD KNOCKDOWNS:	LOCAL	INTER-RING	GENERAL
(ARBOCZ/PANDA2):	NOT COMPUTED	9.6748E − 01	1.0000E + 00
FROM PANDA2 THEORY:	1.0000E + 00	9.4700E − 01	8.7067E − 01
FROM ARBOCZ THEORY:	1.0000E + 00	8.1194E − 01	9.2626E − 01
USED NOW IN PANDA2:	1.0000E + 00	7.8554E − 01	8.7067E − 01

The governing knockdown factor for each type of buckling is set equal to the minimum knockdown factor for that type of buckling, reduced further by (ARBOCZ/PANDA2), which is the ratio of local, inter-ring, and general buckling loads from Arbocz' theory to those from PANDA2 for the PERFECT shell. The ratio (ARBOCZ/PANDA2) is not computed for local buckling in this case because the Arbocz theory does not apply to shallow panels, that is, for normal isogrid (stringer) spacing

Part 2 Redistribution of stress resultants from prebuckling bending of the imperfect shell under the applied loading

Additional resultants (Nx, Ny) in panel skin from global and inter-ring bending of imperfect panel:
Additional axial resultant, $dNx = -9.4461E+02$
Additional hoop resultant, $dNy = -1.3972E+04$
Additional in-plane shear resultant, $dNxy = 8.2939E+02$

Additional axial resultants dNx along webs and flanges of isogrid from global and inter-ring bending of imperfect panel:
Additional Nx at webtip of striffener 1, $dNx = -6.2893E+03$
Additional Nx at webtip of striffener 2, $dNx = -6.2893E+03$
Additional Nx at webtip of striffener 3, $dNx = -1.4806E+04$

Additional Nx in flange of stiffener 1, $dNx = -7.6638E+03$
Additional Nx in flange of stiffener 2, $dNx = -7.6638E+03$
Additional Nx in flange of stiffener 3, $dNx = -1.8042E+04$

Part 3 Knockdown for smeared rings on cylindrical shell [11, Item 509]
Buckling load factor EIGR for $n = 2$, discrete model = 5.4533E − 01
Buckling load factor for "ring": pcrit = 3*EI/r**3/p = 6.2442E − 01
Knockdown factor, general buckling: EIGR/pcrit = 8.7334E − 01

Part 4 General buckling: smeared stiffeners [11, Items 415, 443]
Load Set A: $Nx, Ny, Nxy = -7.0500E+03 \; -1.41000E+04 \; 7.8821E+01$
Load Set B: $Nxo, Nyo, Nxyo = 0.0000E+00 \; 0.0000E+00 \; 0.0000E+00$

EIGGEN =	1.53E + 00	1.53E + 00	2.49E + 00	5.18E + 00	1.00E + 17	1.53E + 00
SLOPE =	0.00E + 00	0.00E + 00	0.00E + 00	0.00E + 00	0.00E + 00	0.00E + 00
MWAVES =	1	1	2	1	0	1
MWAVES =	2	2	3	5	0	2

Buckling load factor before t.s.d. = 1.5301E + 00 After t.s.d. = 1.515
Buckling load factor BEFORE knockdown for smeared stringers = 1.515
Buckling load factor AFTER knockdown for smeared stringers = 1.515
General buckling load factor before and after knockdown:
EIGGEN before knockdown = 1.5151E + 00
Knockdown factor from general modal imperfection = 8.7067E − 01
Knockdown factor for smearing rings on cyl. shell = 8.7334E − 01
EIGGEN after knockdown = 1.1520E + 00

flange) and of the entire stiffener cross section. Examples of these modes of buckling and rolling are given in [2,3] and further discussion about implementation in PANDA2 is supplied in [11] and below in the discussion of the various margins listed in Table 3.

The buckling loads may be computed by more than one model in order to verify results and to provide appropriate knockdown factors to account for anisotropy, inherent unconservativeness in smearing stiffeners (Part 3 of Table 6, for example), the presence of in-plane shear loading, and variation of in-plane loading within the domain that buckles. The effect of transverse shear deformation is accounted for as described in [2].

2.2. Effect of initial imperfections

The effects of two different types of initial geometric imperfections are induced in PANDA2:

1. initial imperfections that have the same shape as the non-axisymmetric general, inter-ring, and local buckling modes of the perfect panel [6], and
2. initial imperfections that have the shape of the axisymmetric general, panel, and local buckling modes of the perfect panel [7,18–21].

PANDA2 computes knockdown factors corresponding to the two types of initial imperfections (non-axisymmetric, axisymmetric) and uses the lowest of these for each mode of buckling (general, inter-ring, local) in its computation of buckling load factors for each design interation. An example is provided in Part 1 of Table 6. No knockdown factor is computed in PANDA2 corresponding to local buckling of the triangular piece of skin between adjacent isogrid members.

The presence of initial general and inter-ring buckling modal imperfections affects all buckling load factors corresponding to general buckling, inter-ring buckling, local shell skin buckling, and buckling and rolling of the stiffeners. This happens for two reasons:

(1) The buckling modal imperfections increase the effective radii of curvature of the cylindrical shell or panel. (Note: The effective radii of curvature are different for general, inter-ring, and local buckling modal imperfections and these radii increase as the shell is loaded because of prebuckling bending.)

(2) An imperfect shell bends as soon as any loading is applied. The prebuckling bending give rise to redistribution of the prebuckling stresses in the various parts of the stiffened shell structure, as described in [6]. Part 2 of Table 6 shows changes in the membrane resultants, N_x, N_y, N_{xy}, caused by prebuckling bending in the form of a general buckling modal imperfection. Of course, the stress constraints are also affected by the presence of initial imperfections in the form of all three buckling modes of the perfect shell: general, inter-ring, and local.

3. Minimum-weight design of isogrid-stiffened panels and shells

3.1. Introduction

The capability to optimize isogrid-stiffened panels and shells has been added to PANDA2. This was done in 1992 but not reported until now except in [7] and in ITEM 122 of the PANDA2 documentation file PANDA2.NEWS [11]. In addition to isogrid stiffeners, the panel or shell may have rings. Constraints on the design are of the same kind as for the other stiffening configurations: general instability, buckling of smeared isogrid members and skin between rings (called “panel” or “inter-ring” buckling), local buckling of the triangular piece of skin between isogrid stiffeners, buckling and rolling of isogrid stiffener segments, ring segments, and maximum stress in each of the different materials introduced in the PANDA2 preprocessor, which is called “BEGIN” (Table 1). The panel skin, isogrid stiffeners, and rings may be of laminated composite materials.

The PANDA2 user chooses which of the problem variables are to be decision variables during optimization and their lower and upper bounds in the PANDA2 processor called “DECIDE”. These are listed in Table 1.

In the isogrid option there is no discretized single skin-stringer inter-ring module analysis (Fig. 22

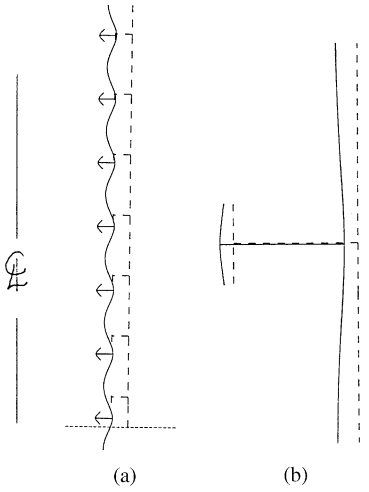

Fig. 1. Axisymmetric prebuckling "hungry horse" deformation of ring stiffened cylindrical shell under uniform external pressure: (a) entire shell, (b) a single module.

of [2]), nor is there a postlocal buckling capability (Fig. 23 of [2]). However, there is a discretized module model that represents one discretized ring and the discretized shell wall (cylindrical skin with smeared stringers or smeared isogrid members) of axial length equal to the ring spacing, as shown in Fig. 1(b). ("Smeared" stiffener models are described in [22]). The root of the ring web coincides with the midlength of the cylindrical shell wall segment. Symmetry boundary conditions are imposed at both ends of the cylindrical shell wall segment, in a manner analogous to the boundary conditions for the skin-stringer discretized modules depicted in [2], for example. The discretized cylindrical shell/ring module model is described in [10].

3.2. Theory

An isogrid pattern of stiffeners is composed of three sets of identical stiffeners, each set spaced a distance b apart and each set oriented at an angle of 60 degrees relative to the other two sets. Hence, the isogrid pattern forms equilateral triangles with height b and side $s = b/0.866$. When smeared out, the isogrid stiffeners form two equivalent isotropic layers:

1. The first equivalent isotropic layer corresponds to the isogrid webs. It has a thickness equal to the height h of the webs and an effective modulus

$$E_{\text{eff}} = E_{\text{web}} t_{\text{web}}/b \tag{2}$$

in which E_{web} is the axial modulus of the web wall, t_{web} is the thickness of the isogrid web, and b is the isogrid spacing.

2. The second equivalent isotropic layer corresponds to the outstanding isogrid flanges. It has a thickness equal to the flange thickness t_{flange} and an effective modulus

$$E_{\text{eff}} = E_{\text{flange}} w_{\text{flange}}/b \tag{3}$$

in which w_{flange} is the width of the outstanding isogrid flange. For composite material

$$E_{\text{web}} = [C_{11\ \text{web}} - C^2_{12\ \text{web}}/C_{22\ \text{web}}]/t_{\text{web}}, \tag{4}$$

$$E_{\text{flange}} = [C_{11\ \text{flange}} - C^2_{12\ \text{flange}}/C_{22\ \text{flange}}]/t_{\text{flange}} \tag{5}$$

in which $C_{ij\ \text{web}}$ and $C_{ij\ \text{flange}}$ are the integrated constitutive coefficients of the web laminate and flange laminate, respectively, and t_{web} and t_{flange} are the web laminate and flange laminate thicknesses, respectively. The Poisson ratio of each of the two smeared out equivalent isotropic isogrid layers is $\frac{1}{3}$ [1]. The isogrid concept was invented by R.R. Meyer et al. of the McDonnell Douglas Company, and the theory on which it is based is set forth in [1].

The theory in PANDA2 represents extensions of the Meyer theory to include laminated composite materials, thermal effects, and local prebuckling bending, such as that called "hungry horse" axisymmetric prebuckling deformation of externally pressurized ring stiffened cylindrical shells, as described in [6] and displayed in Fig. 1(a). A more general local buckling analysis of the triangular piece of skin between isogrid stiffeners is derived to permit calculation of local skin buckling load factors for arbitrary combinations of uniform in-plane resultants N_x, N_y, N_{xy} in the skin and to include the contribution of anisotropic terms from bending–twisting coupling C_{46}, C_{56}. The in-plane skin loads

N_x, N_y, N_{xy} may arise from any combination of applied edge loads N_1, N_2, N_{12}, edge moments M_1, M_2, normal pressure p, and/or thermal loading, as is the case for the other stiffening configurations handled by PANDA2.

The isogrid option in PANDA2 plays the logical role of stringers. In addition to the isogrid stiffeners, the PANDA2 user can add rings. The example given later involves a design with both isogrid stiffeners and rings.

In PANDA2, the local buckling of the panel skin between isogrid members is computed in the TRIANG.NEW library. This library contains the subroutines in which the stiffness A and load-geometric B matrices are set up and the eigenvalue problem

$$Aq = \lambda Bq \tag{6}$$

is solved. The vector q represents the vector of undetermined coefficients, $a_{03}, a_{04}, \ldots, a_{41}$, in Eq. (9). The Ritz method is used. It is assumed that the triangular skin is flat and that only the normal displacement component w and its derivatives play a role. The normal displacement w is expanded in a power series in x and y in the equilateral triangular domain between adjacent isogrid stiffeners. The origin of the x, y coordinate system is located at the midlength of one of the sides s of the equilateral triangle; x lies along s, and y contains the altitude b of the equilateral triangle. Fig. 34 in [7] shows these coordinates.

The following expansion is used for the normal displacement w in the triangular domain bounded by isogrid stiffeners:

$$\begin{aligned} w = {} & a_{01}y + a_{11}xy + a_{02}y^2 + a_{21}x^2y + a_{12}xy^2 \\ & + a_{03}y^3 + a_{31}x^3y + a_{22}x^2y^2 + a_{13}xy^3 + a_{04}y^4 \\ & + a_{41}x^4y + a_{32}x^3y^2 + a_{23}x^2y^3 + a_{14}xy^4 \\ & + a_{05}y^5 + a_{51}x^5y + a_{42}x^4y^2 + a_{33}x^3y^3 \\ & + a_{24}x^2y^4 + a_{15}xy^5 + a_{06}y^6 + a_{61}x^6y \\ & + a_{52}x^5y^2 + a_{43}x^4y^3 + a_{34}x^3y^4 + a_{25}x^2y^5 \\ & + a_{16}xy^6 + a_{07}y^7. \end{aligned} \tag{7}$$

At the boundary of the triangular domain the normal displacement w must be zero. Expression (7) for w satisfies this boundary condition at $y = 0$. The normal displacement w must also be zero at $y = \pm(ax + b)$, where $a = 2b/s$. The boundary conditions

$$w = 0 \quad \text{at } y = \pm(ax + b) \tag{8}$$

can be used to eliminate certain of the a_{ij} in Eq. (7). Tedious algebra is required. The final expression for w, which satisfies the condition that $w = 0$ along all three edges of the equilateral triangle, follows:

$$\begin{aligned} w = {} & a_{03}\{b^2y - 2by^2 + y^3 - 4a^4x^4y^3/b^3 \\ & - 4a^2x^2y^4/b^3 - a^6x^6y/b^4 - 2a^4x^4y^3/b^4 \\ & + 3a^2x^2y^5/b^4\} \\ & + a_{04}\{2b^3y - 3b^2y^2 + y^4 - 9a^4x^4y^2/b^2 \\ & - 11a^2x^2y^4/b^2 - 2a^6x^6y/b^3 \\ & - 6a^4x^4y^3/b^3 + 8a^2x^2y^5/b^3\} \\ & + a_{05}\{3b^4y - 4b^3y^2 + y^5 - 14a^4x^4y^2/b \\ & - 20a^2x^2y^4/b - 3a^6x^6y/b^2 - 11a^4x^4y^3/b^2 \\ & + 14a^2x^2y^5/b^2\} \\ & + a_{06}\{4b^5y - 5b^4y^2 + y^6 - 19a^4x^4y^2 \\ & - 30a^2x^2y^4 - 4a^6x^6y/b - 16a^4x^4y^3/b \\ & + 20a^2x^2y^5/b\} \\ & + a_{07}\{5b^6y - 6b^5y^2 + y^7 - 24a^4bx^4y^2 \\ & - 40a^2bx^2y^4 - 5a^6x^6y - 21a^4x^4y^3 \\ & + 25a^2x^2y^5\} \\ & + a_{13}\{b^2xy - 2bxy^2 + xy^3 - a^4x^5y/b^2 \\ & - 3a^2x^3y^3/b^2 - 2a^4x^5y^2/b^3 \\ & + 2a^2x^3y^4/b^3\} \\ & + a_{14}\{2b^3xy - 3b^2xy^2 + xy^4 - 2a^4x^5y/b \\ & - 8a^2x^3y^3/b - 5a^4x^5y^2/b^2 + 5a^2x^3y^4/b^2\} \\ & + a_{15}\{3b^4xy - 4b^3xy^2 + xy^5 - 3a^4x^5y \\ & - 14a^2x^3y^3 - 8a^4x^5y^2/b + 8a^2x^3y^4/b\} \\ & + a_{16}\{4b^5xy - 5b^4xy^2 + xy^6 - 4a^4bx^5y \\ & - 20a^2bx^3y^3 - 11a^4x^5y^2 + 10a^2x^3y^4\} \\ & + a_{21}\{x^2y - 4a^2x^4y^2/b^3 - 4x^2y^4/b^3 - a^4x^6y/b^4 \\ & - 2a^2x^4y^3/b^4 + 3x^2y^5/b^4\} \\ & + a_{22}\{x^2y^2 - a^2x^4y^2/b^2 - 3x^2y^4/b^2 \\ & - 2a^2x^4y^3/b^3 + 2x^2y^5/b^3\} \end{aligned}$$

$$+a_{23}\{x^2y^3-2x^2y^4/b-a^2x^4y^3/b^2+x^2y^5/b^2\}$$
$$+a_{31}\{x^3y-a^2x^5y/b^2-3x^3y^3/b^2$$
$$-2a^2x^5y^2/b^3+2x^3y^4/b^3\}$$
$$+a_{32}\{x^3y^2-2x^3y^3/b-a^2x^5y^2/b^2+x^3y^4/b^2\}$$
$$+a_{41}\{x^4y-2x^4y^2/b+x^4y^3/b^2-a^2x^6y/b^2\}. \quad (9)$$

The local buckling load factor is computed from the principle of minimum total potential energy. The potential energy consists of the strain energy U_{skin} and the work done W_{skin} by the prebuckling resultants.

N_x, N_y, N_{xy} in the panel skin during buckling modal displacement w. The bending strain energy of the anisotropic flat triangular piece of panel skin is given by

$$U_{\text{skin}}=\frac{1}{2}\int_y\int_x[C_{44}w_{xx}^2+2C_{45}w_{xx}w_{yy}+C_{55}w_{yy}^2$$
$$+4w_{xy}(C_{46}w_{xx}+C_{56}w_{yy}+C_{66}w_{xy})]\,\mathrm{d}x\,\mathrm{d}y \quad (10)$$

and the work done by the uniform prebuckling stress resultants N_x, N_y, N_{xy} in the panel skin is

$$W_{\text{skin}}=\frac{1}{2}\int_x\int_y(N_xw_x^2+N_yw_y^2$$
$$+2N_{xy}w_xw_y)\,\mathrm{d}y\,\mathrm{d}x. \quad (11)$$

The quantities $w_x, w_y, w_{xx}, w_{yy}, w_{xy}$ are found by differentiating the right-hand-side of Eq. (9). Stiffness and load-geometric matrices are computed at an arbitrary point in the triangular domain. Integration is performed numerically, with the trapezoidal rule being used for x-integration and Simpson's rule being used for y-integration.

As seen from Eq. (9) there are 15 degrees of freedom, $a_{03}, a_{04}, \ldots, a_{32}, a_{41}$. The 15×15 eigenvalue problem is solved with use of EISPAC routines. The lowest positive eigenvalue is sought. If there is no positive eigenvalue (which is the case if N_x and N_y are positive and N_{xy} is zero, for example), the local buckling load factor is set equal to a very high number so that no corresponding buckling constraint will be generated.

As the local buckling theory is presently implemented in PANDA2, the 15 degree-of-freedom model in Eq. (9) is used only for analysis types that do not involve optimization (ITYPE $= 2, 3, 4, 5$) because more computer time is required. For optimization (ITYPE $= 1$) a 10 degree-of-freedom model is used, that is, a model that includes all terms in polynomial (7) up to and including sixth order. In all cases run so far, the 10 degree-of-freedom model yields buckling load factors within a few per cent of the 15 degree-of-freedom model. The 10 degree-of-freedom model requires much less computer time than the 15 degree-of-freedom model and is sufficient for the purpose of preliminary design, for which PANDA2 is intended.

Note that for the isogrid configuration there is no local "skin-stringer" module analysis for local prebuckling bending deformation between isogrid stiffeners of the panel skin under uniform pressure. It is assumed that the local stress concentrations from local bending of the panel skin between isogrid stiffeners under pressure are not significant enough to include in the preliminary design of isogrid configurations. The neglect of this type of stress concentration can be compensated for by introduction of a factor of safety for stress that is larger than unity. Also, there is no local skin postbuckling analysis with the isogrid configuration. As mentioned previously, there is no single inter-ring discretized module model involving just the panel skin and the isogrid stiffeners analogous to the discretized "skin-stringer" inter-ring module model shown in Fig. 22 of [2], for example.

4. Numerical example

4.1. Problem definition

Table 1 lists the variable and parameter names and definitions, starting values, which variables are decision variables, lower and upper bounds of the decision variables, equality and inequality constraints, and factors of safety. There are no faying flanges for the stiffeners. The total height of the wall, including the rings, must be less than 2.0 in, and the ring spacing must be greater than three times the isogrid spacing. The width B2(ISO)

of the base of each isogrid stiffener is equal to one-tenth of the isogrid stiffener spacing B(ISO). Since there is no faying flange, this constraint is arbitrary and has no effect on the evolution of the design during optimization cycles.

4.2. Axisymmetric prebuckling behavior

Optimum designs were determined for twelve cases, as listed in Table 2. For the nine cases in which rings are presented PANDA2 optimizes accounting for conditions at two locations: (1) midway between rings, and (2) at the ring stations. The stresses and local buckling load factors are different at these two locations because the perfect ring-stiffened cylindrical shell deforms axisymmetrically under the uniform external pressure as shown in Fig. 1. This deformation is called "hungry horse". It and the prediction of it by PANDA2 are described in [6].

Midway between rings, where the axisymmetric prebuckling deformation bulges inward, the skin of the cylindrical shell and isogrid stiffener set number 3 (oriented circumferentially) are circumferentially compressed more than they are at the ring stations, where there is outward axisymmetric bulging. The outstanding flanges of the internal isogrid stiffener sets 1 and 2 (oriented at +30 and −30 degrees, respectively) at midbay are compressed less than the roots of these stiffeners because of the axisymmetric inward bulging there, whereas the opposite holds at the ring stations.

For example, corresponding to the optimum design listed in Column 1 of Table 2, midway between rings the axisymmetric prebuckling change in axial curvature w_{xx} equals 3.34×10^{-3} in^{-1} and at each ring station w_{xx} equals -7.23×10^{-3} in^{-1}. This prebuckling axial bending gives rise to variation of the compressive axial stress resultant N_x across the heights of the webs of isogrid members 1 and 2:

midbay at the web root : $N_x = -1220$ lb/in,

midbay at the web tip : $N_x = -541$ lb/in,

at rings at the web root : $N_x = -1352$ lb/in,

at rings at the web tip : $N_x = -2819$ lb/in.

The compressive axial stress resultant in the outstanding flanges of isogrid members 1 and 2 are given at midbay by $N_x = -659$ lb/in and at the ring stations by $N_x = -3436$ lb/in. The compressive axial stress resultant in the web of isogrid member 3 is uniform across the height of the web and given at midbay by $N_x = -2698$ lb/in and at the ring stations by $N_x = -2546$ lb/in. For the outstanding flange of isogrid member 3 the midbay and ring station values are $N_x = -3287$ lb/in and $N_x = -3102$ lb/in, respectively. PANDA2 accounts for these variations in prebuckling load in its calculation of maximum effective stress, various buckling load factors for the isogrid stiffeners, and inter-ring buckling of the cylindrical shell. Axisymmetric prebuckling axial bending of the outstanding flange of the ring, evident in Fig. 1, is also accounted for in the computation of the maximum effective stress in the flange at its line of intersection with the web tip. For example, corresponding to the optimum design listed in Column 1 of Table 2, the inner and outer fiber axial stresses in the outstanding flange where it intersects the web are given by PANDA2 as +49 500 and −49 500 psi, respectively.

4.3. Design margins

PANDA2 accounts for a large number of buckling modes and maximum effective stress and equality and inequality constraints during optimization cycles. The various design margins corresponding to these phenomena are listed in Table 3. The top part of Table 3 lists typical design margins corresponding to conditions midway between rings, and the bottom part lists those corresponding to conditions at the ring stations. In PANDA2 jargon "Subcase 1" denotes midbay conditions and "Subcase 2" denotes "at ring station" conditions.

Note: several of the margins listed in the top half of Table 3 apply to the rings even though this section pertains to midbay conditions. Many "ring" margins are accounted for in both Subcases 1 and 2 because of certain strategies introduced into PANDA2 to handle the effect of both positive and negative initial general buckling modal imperfections within a single load set [11].

Table 4 lists the values of the margins corresponding to the optimized geometries listed in

Table 2 for conditions midway between rings. Table 5 lists the same information corresponding to conditions at the ring stations.

Note that each margin definition for buckling listed in Table 3 contains information about the buckling mode, such as number of halfwaves in the axial (M) and circumferential (N or n) coordinate directions. (For buckling of stiffeners M always means "number of halfwaves along the axis of the stiffener".) The stress margins contain information about the location of the maximum effective stress, such as material number, module segment number (see [2]), nodal point number (e.g. $n=6$), layer number, and value of the thickness coordinate z. In the twelve cases listed in Table 2, for which margins are listed in Tables 4 and 5, the values of M, N, z and isogrid member number, isogrid, $i=1,2,3$, will differ from case to case. They will usually not be equal to the specific values that happen to be listed in Table 3, most of which correspond to the results listed in Column 10 of Tables 2, 4 and 5. The purpose of Table 3 is to identify the type of behavior that influences the evolution of the design during optimization of the twelve cases listed in Tables 2, 4 and 5, not to specify the exact form of the margin definition with regard to wavenumbers and locations of maximum effective stress in each of the cases. In this respect, Table 3 is a sample only.

4.4. Explanation of the margins listed in Table 3

Margins 1–4 *in Subcase* 1 *and* 1–5 *in Subcase 2*: These buckling margins are generated by the discretized ring/shell-wall single module models introduced into PANDA2 as described in [10] and depicted in Fig. 2. The consitutive matrix C_{ij} for the shell wall includes smeared stringers (or isogrid members), where "smearing" the stiffeners is accomplished as described in [22]. The buckling load factors and mode shapes for the discretized single module depend on the number n of circumferential waves. In general if one plots the buckling load factor versus n, one obtains a curve that has multiple minima. Each minimum corresponds to a different mode of buckling. For example, the ring/shell module shown in Fig. 2 has three minima. For $n=2$ circumferential waves, there is buckling characterized by sidesway of the ring web; for $n=6$ there is inter-ring buckling; for $n=18$ there is local buckling of the ring web. PANADA2 searches over three ranges of n: a "starting" range, a low-n range, and a high-n range. For any of these ranges in which a minimum buckling load factor vs. n occurs, PANDA2 scans the buckling mode associated with that minimum and classifies the buckling as "inter-ring" if the maximum buckling modal deflection occurs midway between rings (at either the top or bottom of the cylindrical shell shown in Fig. 2a), as "ring sidesway" if the maximum buckling modal deflection occurs at the tip of the ring web, and as "web buckling" if the maximum buckling modal deflection occurs near the midheight of the ring web. The "starting" range of n is determined from the closed-form PANDA-type prediction [3] of inter-ring buckling, listed as Margin No. 16 in the top part of Table 3 and computed as illustrated in Table 7. The low-n range covers all n below the lowest n explored in the "starting" range and the high-n range covers a large range of n for values above the highest n explored in the "starting" range. Buckling margin definitions are constructed by PANDA2 by concatenation of a string that identifies the n-range with a string that identifies the type of buckling. (Note: the "starting" range of n has to identifying n-range string.)

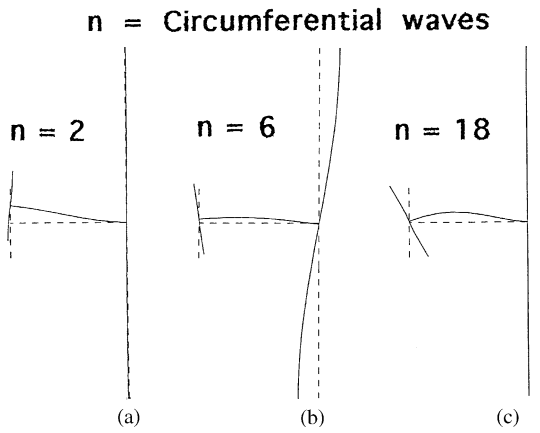

Fig. 2. Buckling modes of a single discretized shell-wall/ring module: (a) ring sidesway, (b) inter-ring buckling, (c) ring web buckling.

Margins 5–7 *in Subcase* 1 *and* 6–8 *in Subcase* 2: In-plane stress components and, in the present case,

Table 7
PANDA2 output for inter-ring buckling corresponding to the optimum design listed in Col. 1 of Table 2 (perfect shell)[a]

Load Set A:	*Nx*,	*Ny*,	*Nxy* = − 7.0500E + 03	−1.4100E + 04	7.8821E + 01		
Load Set B:	*Nxo*,	*Nyo*,	*Nxyo* = 0.0000E + 00	0.0000E + 00	0.0000E + 00		
EIGMNC=	4.29E + 00	4.29E + 00	4.29E + 00	4.78E + 00	1.00E + 17	4.29E + 00	1.31E + 01
SLOPE=	0.00E + 00	0.00E + 00	0.00E + 00	0.00E + 00	0.00E + 00	0.00E + 00	0.00E + 00
MWAVE=	1	1	1	1	0	1	1
MWAVE=	5	5	5	7	0	5	0

Buckling load factor before t.s.d. = 4.2895E + 00 After t.s.d. = 4.0634E + 00
Buckling load factor BEFORE knockdown for smeared isogrid = 4.0634E + 00
Buckling load factor AFTER knockdown for smeared isogrid = 4.0634E + 00

Inter-ring buckling (smeared isogrid) load factor before and after knockdown:
EIGSS (before knockdown by the factor below) = 4.0634E + 00
Knockdown factor, inter-ring modal imperfection = 9.6748E − 01 (ARBOCZ/PANDA2)
After knockdown : = 3.9313E + 00

Simple-support inter-ring buckling with smeared stringers is not recorded as a margin because this type of buckling has been superceded by the results from the discretized inter-ring module model, for which buckling load factors have been computed in the range from $n = 1$ to 32 circumferential halfwaves. The PANDA-type simple-support inter-ring buckling model, results from which are listed above, has 5 circumferential halfwaves, which lies within this range.

[a]The results listed here are obtained from the "PANDA-type" (closed form) model described in [3].

the von Mises effective stress, are computed at the inner and outer surfaces of each layer in the wall of each segment in both the skin/stringer and skin/ring modules. In discretized modules these stress components are computed at multiple nodal points in each segment of the skin/stringer module. In the present case there are four segments in each of the skin/isogrid and skin-with-smeared-isogrid/ring modules. For the skin/isogrid module, segment 1 is the panel skin, segment 2 is the stiffener base (considered by PANDA2 to be part of the panel skin and in the case of isogrid stiffening with properties identical to those of segment 1), segment 3 is the stiffener web, and segment 4 is the outstanding flange. For the skin-with-smeared-isogrid/ring module (Fig. 1b), stresses are computed only in the web and outstanding flange of the ring, which are segments 3 and 4, respectively. Stresses are computed at the root and tip of the web and only at the flange inner and outer surfaces at the point in the flange where the web and flange intersect. PANDA2 finds the maximum effective stress for each different material introduced by the user in the "BEGIN" processor. (There are two materials in the present example: Material 1 for the panel skin and isogrid stiffening and Material 2 for the web and outstanding flange of the ring. These two materials have identical properties. The reasons for introducing two identical materials are given in [7].) The three stress margins in the top part of Table 3 correspond respectively to:

MARGIN 5 The effective stress in the panel skin (isogrid member base) at the line of intersection with the isogrid web on the skin surface opposite to that to which the isogrid web is attached (outer surface of the cylindrical shell in this example).

MARGIN 6 The effective stress at the innermost surface of the outstanding flange of the isogrid member.

MARGIN 7 The effective stress at the innermost surface of the outstanding flange of the ring.

As mentioned previously, the specific locations of the most critical effective stresses might differ in

each of the twelve cases listed in Tables 2, 4 and 5. The list in Table 3 is a sample only.

The present case involves only isotropic materials, for which the number of stress constraints is compressed via the concept of a single von Mises effective stress and the fact that there is no difference in the material failure criterion for tensile and compressive effective stress. Therefore, adding an additional material in order to capture different stress constraints for different parts of the structure does not result in a great increase in the number of constraint conditions present during optimization.

In the case of composite materials, however, it may not be possible to specify multiple materials that are in fact the same. This is because each composite material generates five different stress constraints: maximum tension along the fibers, maximum compression along the fibers, maximum tension normal to the fibers, maximum compression normal to the fibers, and maximum in-plane shear. If there are several load cases and subcases, the total number of constraints can become larger than that allowed by PANDA2 as it is presently written (99 behavioral constraints).

Margins 8–10 *in Subcase* 1 *and* 9–11 *in Subcase* 2: These isogrid web buckling margins are derived from the theory described in ITEMs 121 and 120d of PANDA2.NEWS [11]. The terms "isogrd1", "isogrd2", "isogrd3" means isogrid stiffener set no. 1, 2, 3, respectively. The buckling load factors are calculated with the assumption that each web is simply supported along its two longitudinal edges, that is, along the lines of intersection with the skin and with the outstanding flange. The linear variations of the axial resultant over the heights of the webs, generated because there is prebuckling "hungry horse" bending and possibly initial geometric imperfections that give rise to prebuckling bending, are accounted for, as described above. The presence of transverse compression in the web of stiffener "isogrd3" is accounted for via a knockdown factor derived as described in ITEM 120d of PANDA2.NEWS [11]. The critical number of local halfwaves along the web axis is determined by searching for the minimum buckling load factor with respect to this number of halfwaves. The length of web considered is B(ISO)/0.866, that is, the length of one side of the equilateral triangle formed by adjacent isogrid stiffeners. The webs of the various isogrid members are assumed to be simply supported where these members intersect. In the sample listed in Table 3, the critical buckling modes have three halfwaves over the distance B(ISO)/0.866 for the webs of isogrid members 1 and 2 and two halfwaves for the web of isogrid member 3. As seen from Tables 4 and 5 "isogrd3" has the most critical web buckling load factor (except in Column 8 of Table 5) because it runs circumferentially and therefore "sees" the full hoop compression $N_y = pR$ from the hydrostatic loading and because the outstanding flange of this particular isogrid member generates transverse compression in the web as the wall of the cylindrical shell moves radially inward under the hydrostatic compression. In Column 8 it is seen that isogrid members 1 and 2 are more critical than member 3. This results from the local prebuckling "hungry horse" bending at the ring station (Fig. 1), which in this one case produces more average compression in the isogrid web of members 1 and 2 than does the overall hoop compression $N_y = pR$ in isogrid member 3.

Margin 11 *in Subcase* 1 *and Margin* 12 *in Subcase* 2: These flange buckling margins are computed from the theory described in ITEMS 121 and 120d of PANDA2.NEWS [11]. The number of halfwaves along the length B(ISO)/0.866 is estimated from the ratio length/height of the web to which the outstanding flange is attached, modified by the square root of the ratio of the web bending stiffness in the transverse (height) direction to that in the length direction. In Subcase 1 only the margin for "isogrd3" is computed rather than margins for all three members, "isogrd1", "isogrd2", and "isogrd3", because PANDA2 determines that the flange with the maximum compressive axial resultant (considered to be uniform across the width of the flange) is that in isogrid stiffener no. 3. In Subcase 2 the outstanding flange of isogrd2 has the most compression. Anisotropy is accounted for, as described in ITEM 121 of PANDA2.NEWS [11]. The minimum buckling load factor with respect to slope of the nodal lines in the buckling mode is determined by a search.

Margin 12 *in Subcase* 1 *and Margin* 13 *in Subcase* 2: The "Isegs 3+4" buckling mode is characterized by participation of both web and outstand-

ing flange, but the line of intersection of web and flange does not translate. (See Fig. 5 on p. 546 of [3].) This margin is derived as described in ITEMS 30 and 516 of PANDA2.NEWS [11]. It is assumed that the axial resultant is uniform over the height of the web. For each of the three isogrid members, a search over the number of axial halfwaves M is conducted. The minimum buckling load factor is selected for the margin. Only one margin is generated, that for the most critical isogrid member. In the Table 3 sample, the critical number of halfwaves over the stiffener length B(ISO)/0.866 is three for both Subcases 1 and 2 (Tables 4 and 5, respectively.) However, in Subcase 1 isogrd3 is most critical, whereas in Subcase 2 isogrd2 is most critical.

Margin 13 *in Subcase* 1 *and Margin* 14 *in Subcase* 2: The buckling mode is a stiffener rolling mode similar to that depicted in Fig. 6(b) of [3], except that the web is assumed to be hinged rather than clamped at its root. The buckling load factor is computed from a Ritz method in which the following functions are assumed for the normal displacement w in the web and flange of an isogrid member:

$$w_{\text{web}} = (as + cs^3)\sin(m\pi x/L),$$

$$w_{\text{flange}} = (a + 3ch^2)s\sin(m\pi x/L) \qquad (12)$$

in which S is the local widthwise coordinate in the web and flange, as shown in Fig. 9 on p. 492 of [2]; h is the height of the web; L is the length of stiffener being considered for buckling ($L = \text{B(ISO)}/0.866$ in this case); and m is the number of buckling modal halfwaves over the length L. The fact that the axial resultant in the web may vary linearly over the height of the web is accounted for. Anisotropic effects (for example, from the C_{46} and C_{56} terms in the integrated constitutive relation) are neglected. The buckling load factor is computed by minimization of the total potential energy with respect to the undetermined coefficients a and c in Eqs. (12) and setting the determinant of the resulting linear homogeneous equations equal to zero. Buckling load factors from this model agree reasonably well with those computed from a BOSOR4 branched shell model of a T-shaped stiffener. These computations are performed for each of the three isogrid members and for a range of m. In general there is more than one minimum in the array of buckling load factor versus m. As with the previous margin ("Isegs 3+4"), PANDA2 finds in the sample case to which Table 3 corresponds that isogrd3 is the most critical at midbay and isogrd2 is most critical at the rings.

Margin 14 *in Subcase* 1 *and Margin* 15 *in Subcase* 2: Margin 14 in Subcase 1 (ring web buckling) is analogous to Margins 8–10 in Subcase 1 and Margin 15 in Subcase 2 is analogous to Margins 9–11 in Subcase 2. The theory is the same and the buckling load factors are computed by the same subroutine. The number of local halfwaves is large, 21 in this sample, because the effective length over which ring web buckling can occur is assumed to be the entire width of the panel (πR) rather than the distance between intersection points of the ring webs with the isogrid stiffeners. The entire width of the panel is used because the webs of the rings might be considerably higher than the webs of the isogrid stiffeners and deformation of them is therefore not much constrained by intersections with the isogrid members.

Margin 15 *in Subcase* 1 *and Margin* 18 *in Subcase* 2: If the outstanding flange of a stiffener is highly compressed and if it is supported on a web that is relatively soft in its transverse (height) direction, then the flange might buckle as a beam on an elastic foundation. The elastic foundation is the support provided by the web. This margin is derived as described in ITEM 383 in the PANDA2.NEWS file [11]. It is critical only in the extreme case listed in Column 10 in Tables 4 and 5. (Column 10 represents a design that is very far from being feasible, as will be described later.)

Margin 16 *in Subcase* 1: This inter-ring buckling margin is computed from PANDA-type theory (see Eq. (57), p. 553 of [3]) with use in this particular sample of Sanders theory [7,23,24]. The isogrid members are smeared out [22] and the buckling mode is "panel" buckling between adjacent rings (inter-ring buckling). The shell is assumed to be simply supported at the ring stations in the buckling analysis, and the rings are ignored in the buckling phase of the computations. In this sample there is one halfwave in the axial direction ($M = 1$) between rings and six halfwaves in the circumferential direction ($N = 6$ over the circumferential arc length, πR). Note that this margin does not show up

in any of the cases listed in Table 4 because it is always superceded in this particular study by margins generated from the discretized ring/shell-wall single module model described above and represented in Fig. 2. More is written on this strategy later in connection with Table 7.

Margin 17 *in Subcase* 1: This general buckling margin is computed from PANDA-type theory (See Eq. (57), p. 553 of [3]) with use of the Sanders theory [7,23,24] in this example. There is one halfwave in the axial direction ($M = 1$) over the entire length of the shell and two halfwaves in the circumferential direction ($N = 2$). In the general instability model of buckling, both isogrid stiffeners and rings are smeared out [22]. If the Donnell theory had been used rather than the Sanders theory, results from the Donnell theory, which is known to be unacceptably unconservative for buckling of cylindrical shells under external pressure if the critical number of circumferential waves n is three or less, would have been "knocked down" by the ratio $(n^2 - 1)/n^2$ in order to compensate for the Donnell shallow shell approximation. In this particular study it turns out that the factor $(n^2 - 1)/n^2$ is too conservative.

Margin 18 *in Subcase* 1 *and Margin* 19 *in Subcase* 2: The stiffener rolling buckling mode is analogous to that shown in Fig. 6(b) on p. 546 of [3]. The web is assumed to be clamped at its root, and any variation of resultant over the height of the web is neglected. Anisotropic effects are neglected. The critical mode in this particular sample has one halfwave ($M = 1$) over the length B(ISO)/0.866. Isogrid member no. 3 is the most critical midway between rings and isogrid member no. 2 is the most critical at the rings. Rather than compute isogrid rolling margins for all three sets of isogrid stiffeners, PANDA2 identifies the most critical set as the same as that determined in connection with Margin no. 13 of Subcase 1 and Margin no. 14 of Subcase 2 because these earlier margins represent a similar stiffener rolling phenomenon.

Margin 19 *in Subcase* 1 *and Margin* 20 *in Subcase* 2: There may be more than one minimum in the array of stiffener rolling load factors versus number of axial halfwaves M. If PANDA2 detects a double minimum, it constructs a new stiffener rolling margin containing the string "hiwave" corresponding to the minimum at the higher number of halfwaves along the stiffener axis. The critical "hiwave" mode in this particular sample has three halfwaves ($M = 3$) over the length B(ISO)/0.866.

Margin 20 *in Subcase* 1 *and Margin* 23 *in Subcase* 2: The axisymmetric ring buckling mode is of the type shown in Fig. 2a. The buckling load factor is computed as described in [3]. A factor of safety, FS = 1.6, is automatically supplied by PANDA2 as a result of a history of comparisons with predictions from BOSOR4 [4].

Margin 21 *in Subcase* 1 *and Margin* 24 *in Subcase* 2: This isogrid web buckling margin represents essentially the same behavior as that computed in connection with Margins 8–10 in Subcase 1 and Margins 9–11 in Subcase 2 except that here the buckling load factor is computed including the effect of in-plane shear loads in the web (Eq. (57) of [3]) and neglecting the effect of variation of compression over the height of the web.

Margin 22 *in Subcase* 1 *and Margin* 25 *in Subcase* 2: These ring web buckling margins are analogous to Margin 21 in Subcase 1 and Margin 24 in Subcase 2, except that they pertain to the ring web instead of the stringer (isogrid) web. The number of halfwaves, $M = 15$, is fairly large because the effective circumferential arc length is taken to be πR rather than the spacing between isogrid stiffeners.

Margin 23 *in Subcase* 1 *and Margin* 26 *in Subcase* 2: This skin buckling margin is computed in the new library TRIANG.NEW as described in connection with Eqs. (7)–(11). Derivation of the theory to obtain this local buckling factor constituted most of the work of generating the new isogrid capability discussed in this paper. Observe from a comparison of Tables 4 and 5 that the local triangular skin buckling load factors are higher for Subcase 2 than for Subcase 1. This is because the prebuckling axisymmetric "hungry horse" axial bending (Fig. 1) creates more compression in the internally stiffened skin midway between rings than at the rings.

Margin 24 *in Subcase* 1: This maximum strain margin, not at all critical in this case, is included to allow the user to account for strain concentrations created by fasteners or other structural characteristics for which the strain concentration is known to be a certain multiple of the average strain.

Margin 25 *in Subcase* 1: This inequality margin prevents the stringer (or isogrid) base width

from getting too large. It is not relevant in this case of isogrid stiffening for which no faying flanges are permitted in the isogrid members. This inequality constraint is created by PANDA2, not by the PANDA2 user. Its value is always equal to 2.33 in the cases presented here because the PANDA2 user has specified in the DECIDE processor that B2(ISO) = 0.1 × B(ISO) (see Table 1).

Margin 26 *in Subcase* 1: This inequality margin represents the geometric inequality constraint that the total height of the shell wall, including rings, must not exceed 2.0 in. The inequality constraints are introduced by the PANDA2 user in DECIDE.

Margin 27 *in Subcase* 1: This inequality margin represents the geometric inequality constraint that the ring spacing B(RNG) must be greater than three times the isogrid spacing B(ISO).

Margins 16, 17, 21, 22 *in Subcase* 2: These four ring buckling margins do not appear in Subcase 1, so they have not yet been discussed. Margin 16 is analogous to Margin 12 in Subcase 2, except that this is the outstanding flange of a ring and not that of an isogrid stiffener. The effective length of stiffener is taken to be the entire width πR of the panel. The number of circumferential halfwaves in the buckle pattern is taken to be the same as that of the ring web to which the flange is attached (Margin 15). Margin 17 is analogous to Margin 13, except that this is a ring and not an isogrid stiffener. Margin 21 is analogous to Margins 19 and 22 is analogous to Margin 20. With Margins 21 and 22 the number of halfwaves along the ring axis is called N instead of M, which is inconsistant with the nomenclature used in Margin 25.

4.5. SUPEROPT optimization of the perfect stiffened cylindrical shell

This discussion pertains to Column 1 of Tables 2, 4 and 5. A "global" optimum design was found by means of four successive executions of SUPEROPT, each SUPEROPT followed by an execution of PANDA2 processors called "CHOOSEPLOT" and "DIPLOT" in order to obtain the plots shown in Figs. 3(a)–(d). The starting design at the beginning of each execution of SUPEROPT is the best (lightest almost feasible) design determined during all the previous executions of SUPEROPT.

In the first execution of SUPEROPT the modified Donnell shallow shell theory was used. (By modified is meant the Donnell theory prediction multiplied by the factor $(n^2 - 1)/n^2$ in which n is the number of circumferential halfwaves over the 180-degree arc of the panel. This factor compensates for the generally unconservative predictions from Donnell theory for buckling of externally pressurized cylindrical shells the critical buckling mode of which has few circumferential waves.)

In Fig. 3(a) the spikes at Iterations 30, 60, 90, 120, 150, 180, 210, 240, and 270 correspond to new starting designs generated by means of Eq. (1). Following each application of Eq. (1), the main processor of PANDA2, called "PANDAOPT", is executed five times, leading to locally converged values of the objective that vary between 27.5 and 28.5 lbs. Although the nine locally minimum values of the objective do not differ from each other by much, the corresponding nine locally optimum designs are quite different from each other. For example, at Iterations 30, 60, 90, 120, 150, 180, 210, 240, and 270, the isogrid spacing B(ISO) converges approximately to 1.2, 1.7, 1.7, 1.7, 2.5, 2.2, 2.0, 2.6, and 2.5 in, respectively. The ring spacing B(RNG) converges approximately to 5.0, 5.0, 5.0, 5.0, 8.0, 6.5, 6.0, 7.8, and 7.5 in, respectively. The isogrid web height and flange width and various thicknesses exhibit similar variation.

Figs. 3(b)–(d) were generated with the Sanders theory [23,24] used instead of the modified Donnell theory.

As seen from Figs. 3b and 3c, the results from the second and third executions of SUPEROPT display non-convergent behavior after Iteration 25 in Fig. 3(b) and after Iteration 100 in Fig. 3(c). The objective oscillates from iteration to iteration and drifts away from the optimum value of approximately 25 lbs. Figs. 4 and 5, which correspond to Fig. 3b, help to explain what happens. Between Iterations 30 and 80, while the objective remains constant in an average sense and not too far above the minimum value of 25 lbs, the ring web height and flange width become very small (Fig. 4). As seen from Fig. 5 there are many critical margins during these iterations. Therefore, PANDA2 senses the nearby presence of an optimum design and has difficulty leaving this region of design space. For Iterations

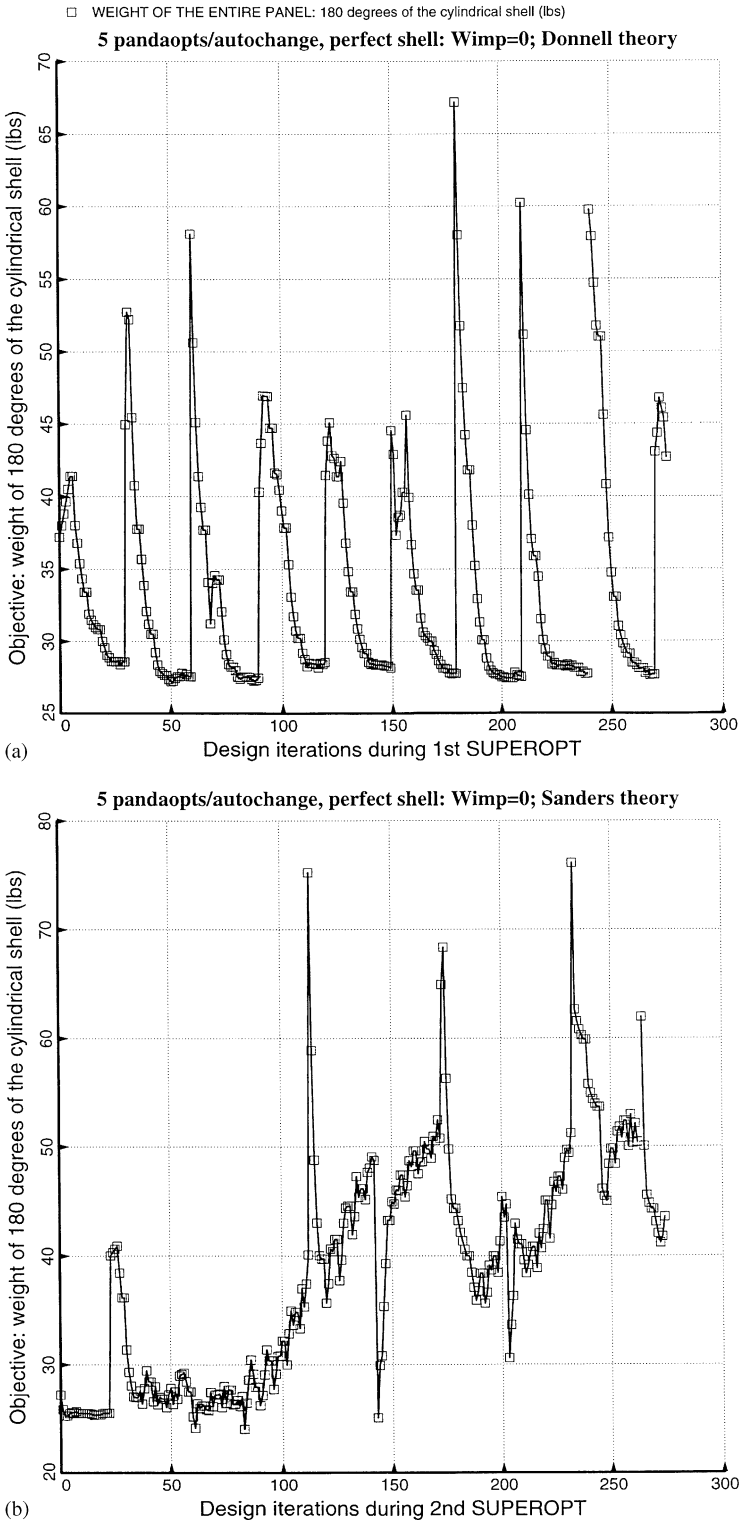

Fig. 3. Global optimization of perfect isogrid and ring stiffened shell: (a–d) after execution of 1–4th SUPEROPT.

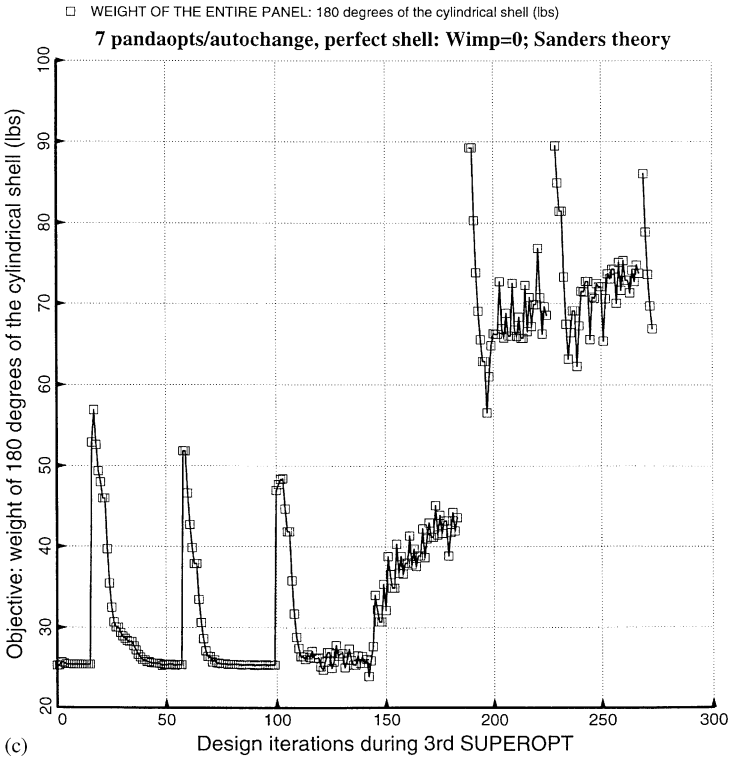

(c)

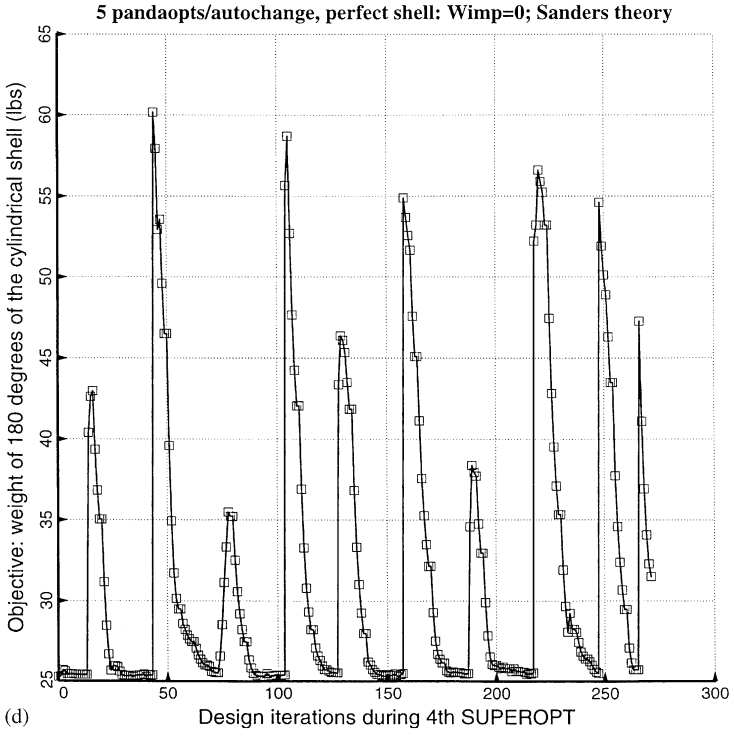

(d)

Fig. 3. (*Continued*).

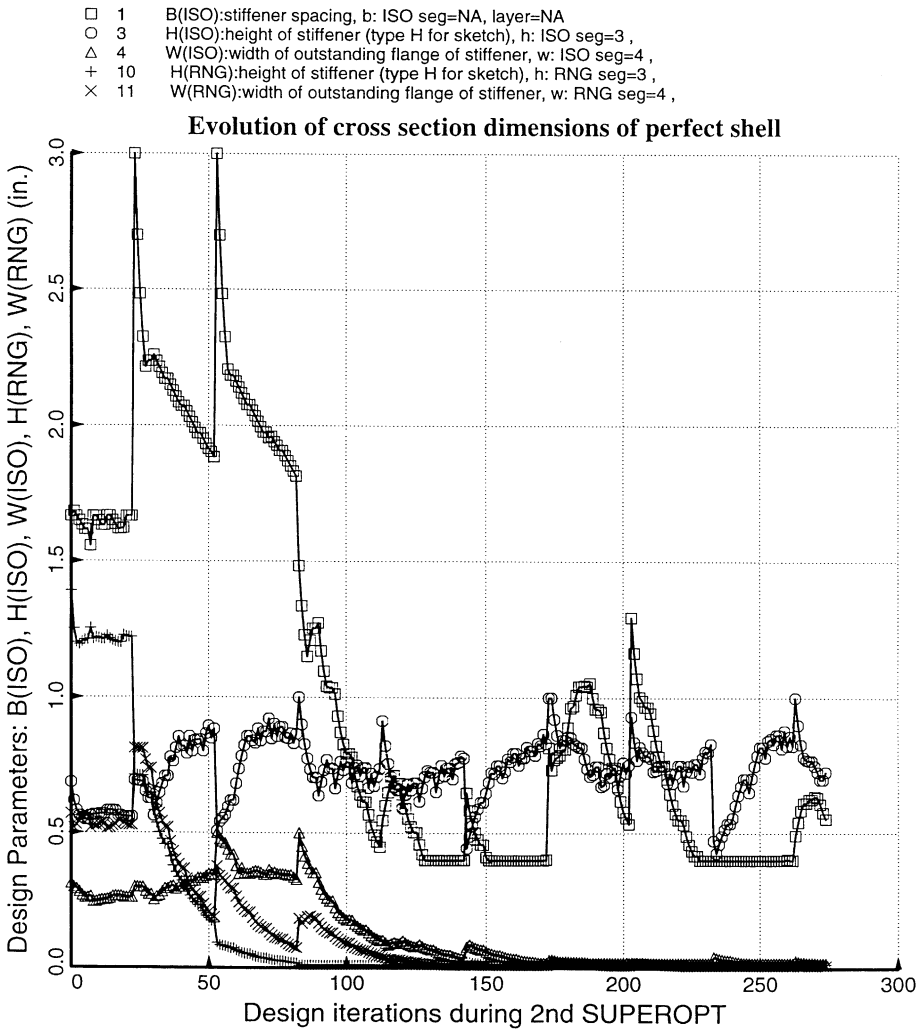

Fig. 4. Evolution of isogrid and ring cross sections during the 2nd SUPEROPT.

80 and above, the objective drifts upward at first and then wanders between 40 and 50 lbs (Fig. 3b). The rings disappear for all practical purposes, the outstanding flange of the isogrid stiffeners disappears, and the isogrid spacing approaches its lower bound. There are still several critical margins, and PANDA2 has difficulty keeping the general buckling margin in positive territory. However, there do exist almost feasible designs (at about Iteration 175 and again at about Iteration 230), so that PANDA2 cannot seem to escape from this unproductive region of design space.

Much of the difficulty stems from the very small lower bounds set on many of the decision variables (Table 1). It is possible that each new starting design produced via Eq. (1) can include one or more decision variables that are very small. Once this happens, it is difficult for that variable or those variables to increase by an order of magnitude while PANDA2 continues to encounter feasible or almost feasible designs in the presence of several critical margins.

Fig. 3(d) exhibits a return to the more productive pattern of exploration shown in Fig. 3(a). The au-

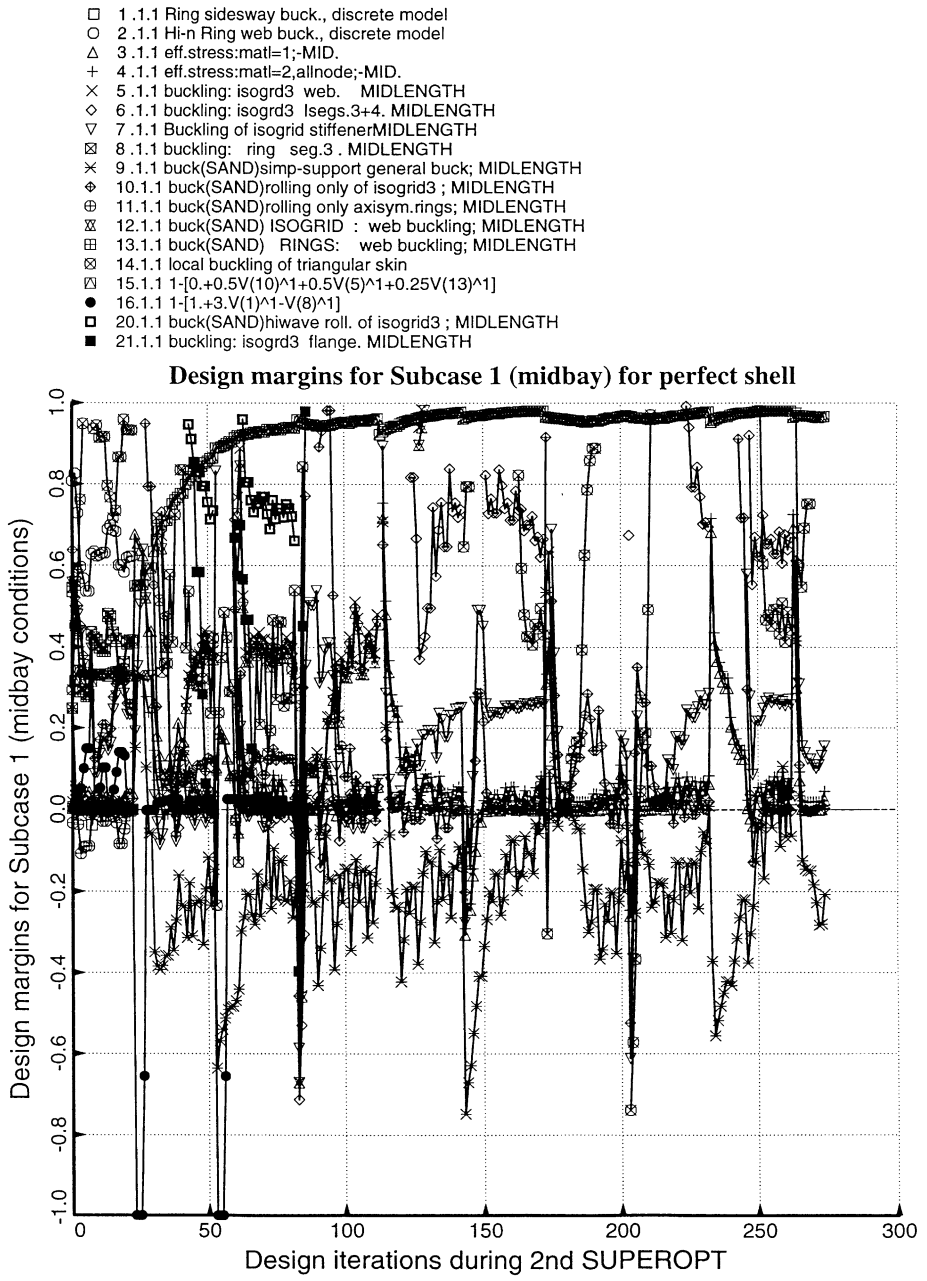

Fig. 5. Evolution of midbay margins during the 2nd SUPEROPT.

thor rather arbitrarily decided to accept the "globally" best design after the four executions of SUPEROPT rather than continuing with more SUPEROPTs. That design is listed is Column 1 of Table 2. The values of the corresponding margins are listed for midbay conditions in Column 1 of Table 4 and for "at ring" conditions in Column 1 of Table 5. Note that the optimum ring spacing listed in Column 1 of Table 2 is 57.38 in and the optimum weight is 25.29 lbs. However, the design listed

in Column 2 of Table 2, for which the ring spacing B(RNG) was held constant at 5.0 in during optimization, is slightly lighter, weighing 25.21 lbs. PANDA2 failed to find this design during the many, many iterations of the four SUPEROPTs that produced the Column 1 design. However, the improvement is not significant, and it is unlikely that there exists a feasible or almost feasible design that is significantly lighter than those listed in Columns 1 and 2 of Table 2. Although the optimum weights listed in Columns 1 and 2 are very close, the two corresponding optimum designs are quite different.

4.6. Discussion of other cases involving perfect shells

The designs listed in Columns 2–6 in Table 2 were obtained after multiple executions of SUPEROPT with the ring spacing removed from the vector of decision variables and fixed at five different values. Note that the optimum weights are almost constant. Even the optimized perfect shell without any rings (Column 7) is only about six per cent heavier than the optimized perfect shell with rings spaced at 5.0 in. The presence of the stress constraint causes the skin and isogrid stiffeners to become heavy enough that adding rings does not provide much improvement. If the stress constraint is removed (Columns 8 and 9) the optimized shell with rings is significantly lighter than that without. Note, however, that the design listed in Column 8 is not practical because there are very high stresses.

Retention of the rings and the stress constraints and removal of the isogrid leads to an optimum design which is significantly heavier than that with the isogrid, weighing 33.80 lbs compared to 25.21 lbs. (See the second-to-last line in Table 2.) Hence, the perfect shells the isogrid is significant and the rings are not especially significant.

4.7. Imperfect shells

Columns 10–12 pertain to shells with a general buckling modal imperfection of amplitude 0.094 in, one per cent of the shell radius. Column 10 lists the same design as Column 1. With the imperfection present the design optimized for the perfect shell is not feasible for reasons described previously (larger local effective radius of the imperfect shell and increased stresses caused by prebuckling bending). Columns 10 in Tables 4 and 5 contain many very negative buckling and stress margins.

Column 11 lists the optimum design of the imperfect shell. It is significantly heavier than the optimized perfect shell, 37.36 lbs compared to 25.21 lbs. Optimization without any rings (Column 12) demonstrates that, in contrast to the situation for the perfect shell, rings are important for an imperfect shell. On the other hand, as demonstrated by the last line in Table 2, for the imperfect shell the isogrid stiffening is not very important. With the isogrid stiffening the imperfect optimized shell weighs 37.36 lbs compared to 38.30 lbs for the imperfect optimized shell without isogrid stiffening.

Hence, a designer who bases his decision on whether or not to include isogrid stiffening on predictions of stress and buckling of perfect shells might well come to a conclusion opposite to that of a designer who bases his decision on the behavior of an imperfect shell, at least for the parameters used in the cases studied here.

4.8. Absence of an inter-ring buckling margin in Table 4

For all the cases listed in Table 4 (midbay conditions) there is no Margin No. 16, "simple-support inter-ring buckling". This type of buckling is computed in PANDA2 as listed in Table 7, which corresponds to the optimum design listed in Column 1 of Table 2. After the thorough search in (m, n, slope) space as described previously in connection with general buckling, PANDA2 finds a minimum buckling load factor of 4.29 for interring buckling with one halfwave in the axial direction (between rings) and five halfwaves over the 180-degree circumferential arc. In this PANDA-type closed form model [3] it is assumed that the panel is simply supported at the ring stations and the rings are not accounted for during computation of buckling load factors. For this geometry, the BOSOR4 program [12] obtains a buckling load factor of 4.42 with the same critical mode shape as that predicted by PANDA2.

In the PANDA2 computations the load factor, 4.29, is knocked down to 4.06 to account for transverse shear deformation (t.s.d.), and further

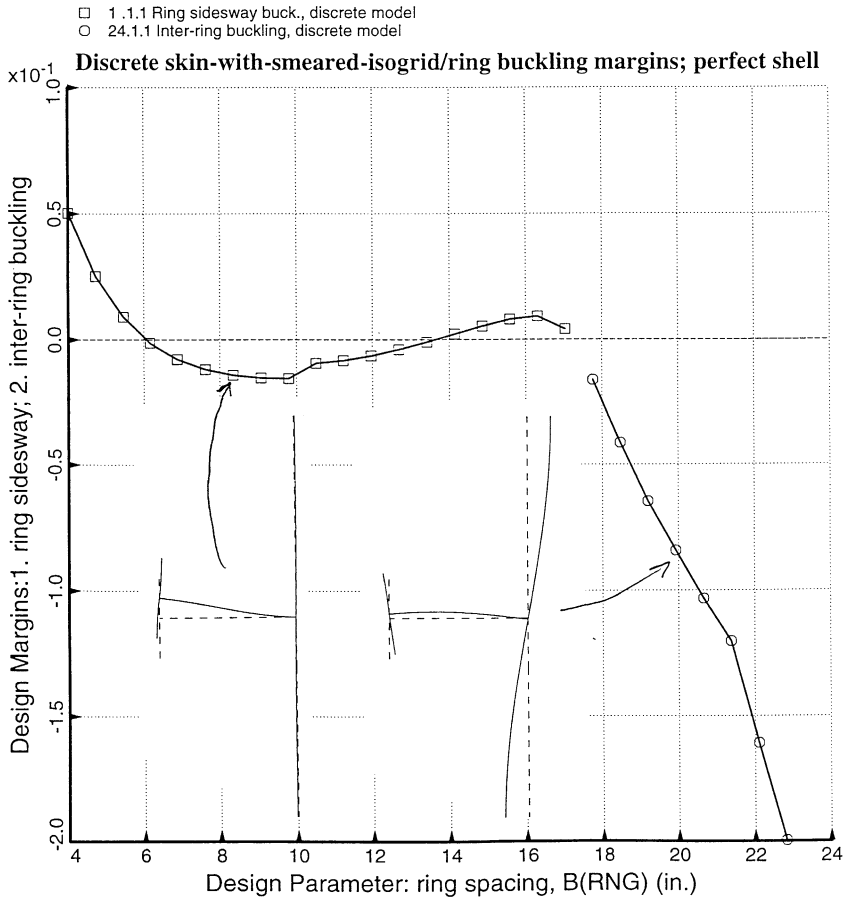

Fig. 6. Buckling margins from single discretized shell-wall/ring module corresponding to the optimized perfect shell design listed in Col. 1 of Table 2.

knocked down by the "ARBOCZ/PANDA2" factor, 0.967, as explained in Part 1 of Table 6. The paragraph at the end of Table 7 explains why the margin corresponding to this PANDA-type inter-ring buckling load factor is not included with the other margins: it is superceded by the more elaborate discretized ring/shell-wall module model displayed in Fig. 2 and described in connection with Margins 1–4 at the top of Table 3 and Margins 1–5 at the bottom of Table 3 and in [10].

Fig. 6 shows margins from the discrete ring/shell-wall module model for ring spacing from 4.0 to 23.0 in. The other dimensions are those listed in Column 1 of Table 2. For ring spacing less than 17 in the critical buckling mode corresponds to ring sidesway. For higher ring spacing the critical mode corresponds to inter-ring buckling. At the optimum design listed in Column 1 of Table 2 the ring spacing is 5.738. Therefore, the inter-ring type of buckling is not even close to being critical.

4.9. BOSOR4 predictions of general buckling of perfect shells

Fig. 7 shows general buckling modes and load factors from BOSOR4 models corresponding to the optimum designs listed in Columns 2–6 of Table 2. In every case PANDA2 predicts general buckling with two circumferential waves. BOSOR4 predictions of the critical number of circumferential waves

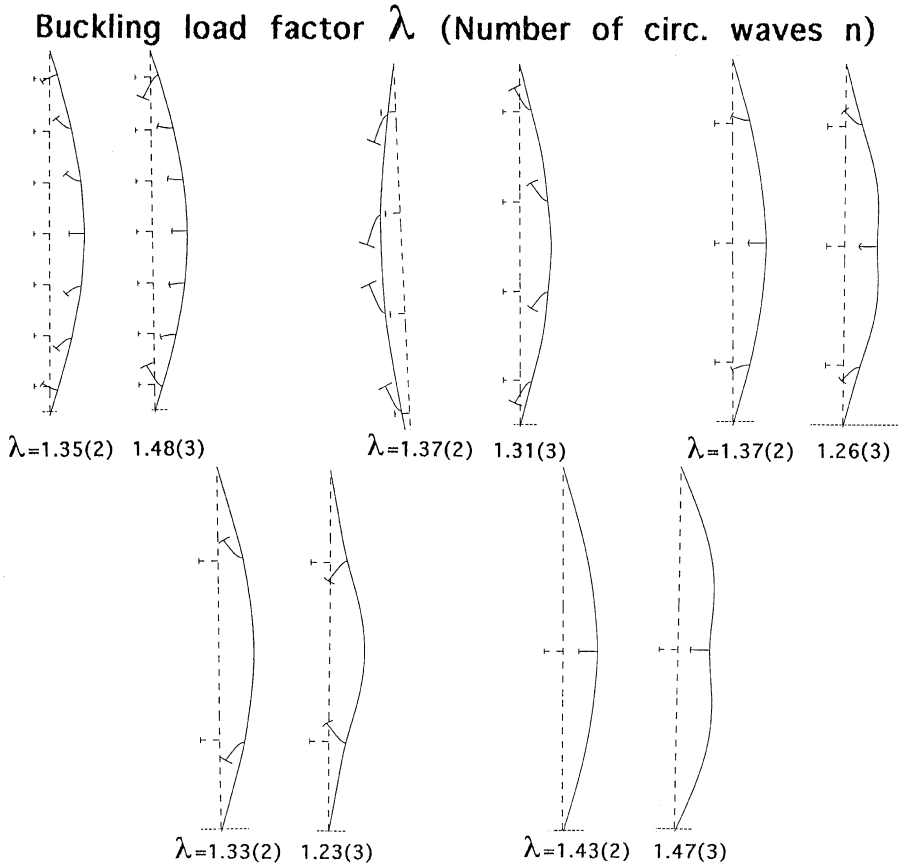

Fig. 7. General buckling of optimized perfect shells as predicted by BOSOR4.

agree for the shell with seven rings and the shell with one ring. For the shells with four, three, and two rings BOSOR4 predicts critical general buckling with three circumferential waves at a load factor slightly lower than that predicted with PANDA2. For the two-ring case, which exhibits the largest discrepancy, PANDA2 produces a general buckling margin of -0.0195 (see Column 5, Margin 17 in Table 4). The factor of safety for general buckling is 1.333 (Table 1). Margins are given by the following expression:

$$\text{Margin} = [(\text{buckling load factor})/(\text{factor of safety}) - 1].$$

Therefore, the buckling load factor from PANDA2 for general buckling is equal to 1.307, about six per cent above the load factor 1.23 from BOSOR4. The discrepancy is caused by the way in which PANDA2 computes a knockdown factor to compensate for the inherent unconservativeness of smearing the rings. The derivation of this knockdown factor is explained in Part 3 of Table 6. In this computation it is assumed that the general buckling mode has two circumferential waves. A smaller knockdown factor would doubtless have been computed for $n = 3$ waves.

4.10. Design sensitivity of optimized perfect and imperfect shells

Figs. 8 and 9 illustrate design sensitivity of the optimized perfect (Column 1) and imperfect (Column 11) shells with respect to the shell wall

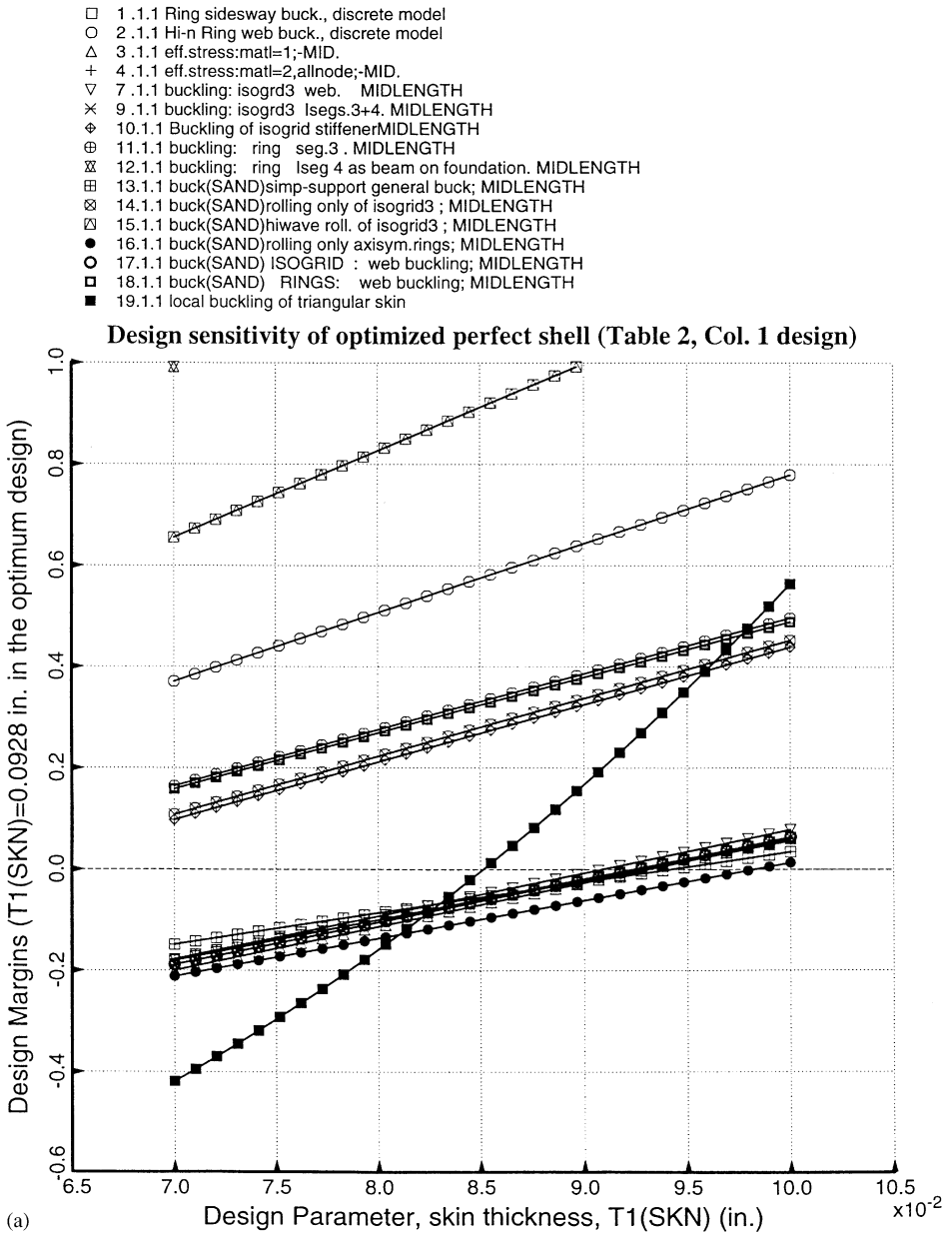

Fig. 8. Design sensitivity of optimized perfect shell: (a) midbay conditions with respect to skin thickness, (b) "at ring" conditions with respect to isogrid spacing.

thickness T1(SKN) (Figs. 8(a), 9(a)) and the isogrid spacing B(ISO) (Figs. 8(b), 9(b)). These plots were generated from an ITYPE = 4 analysis type with PANDA2. As seen from Fig. 8(a) a tight cluster of midbay margins is critical at the optimum value of T1(SKN) = 0.0928 in for the perfect shell. There is less clustering in the case of the optimized imperfect shell at the optimum

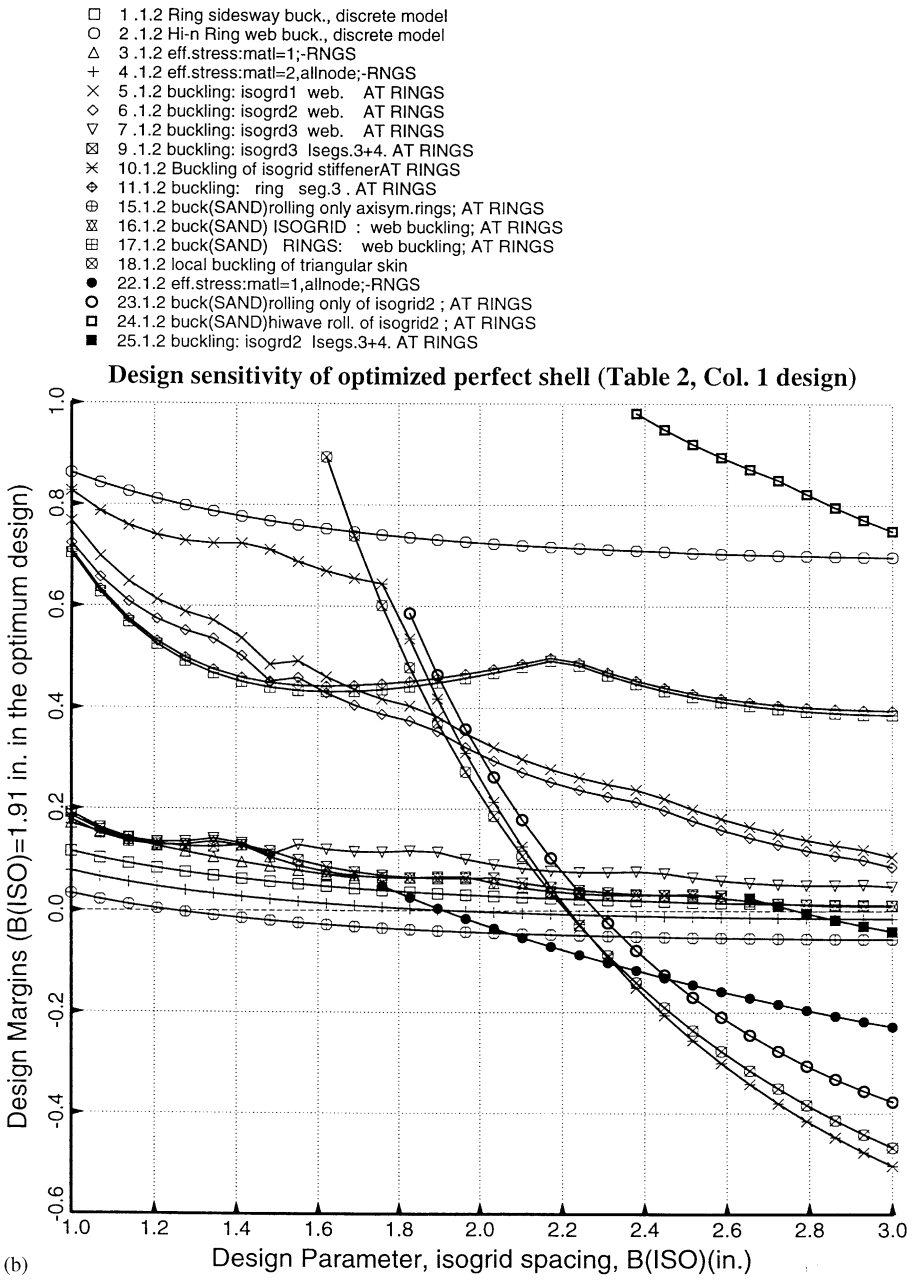

(b)

Fig. 8. (*Continued*).

skin thickness, T1(SKN) = 0.108 in (Fig. 9(a)). The change in clustering from perfect to imperfect shells is less evident in the case of the "at rings" margins (Figs. 9(a) and (b)), presumably because the "hungry horse" prebuckling axial bending gives rise to earlier buckling of the isogrid members 1 and 2 at the ring station than is the case at midbay; the buckling behavior is more complex at the rings

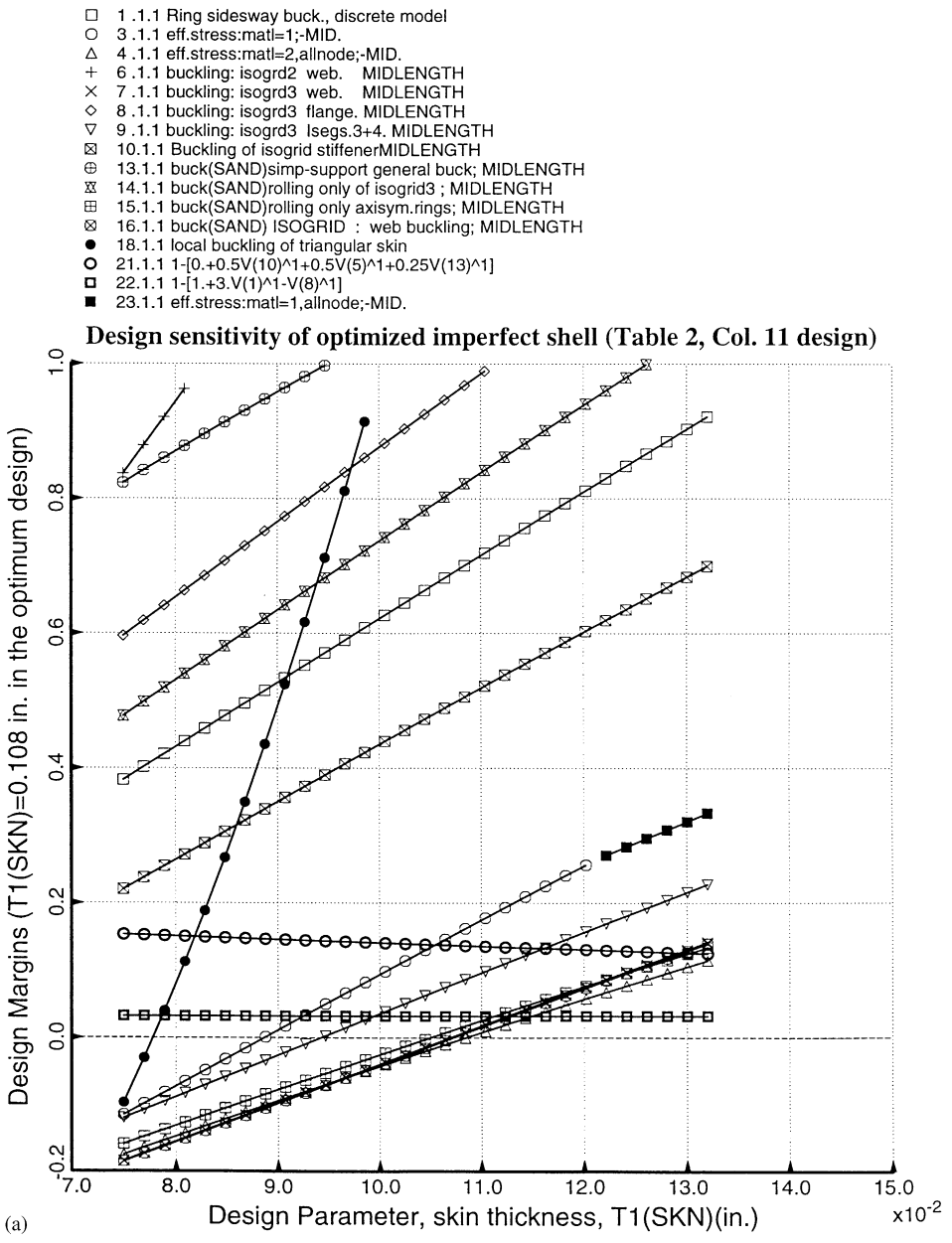

Fig. 9. Design sensitivity of optimized imperfect shell: (a) midbay conditions with respect to skin thickness, (b) "at ring" conditions with respect to isogrid spacing.

than at midbay and this complexity is not diminished by the presence of the imperfection in this particular case. The abrupt changes in the margin for buckling of the flange of isogrd2 in Fig. 9(b) are caused by changes in the number of waves in this buckling mode.

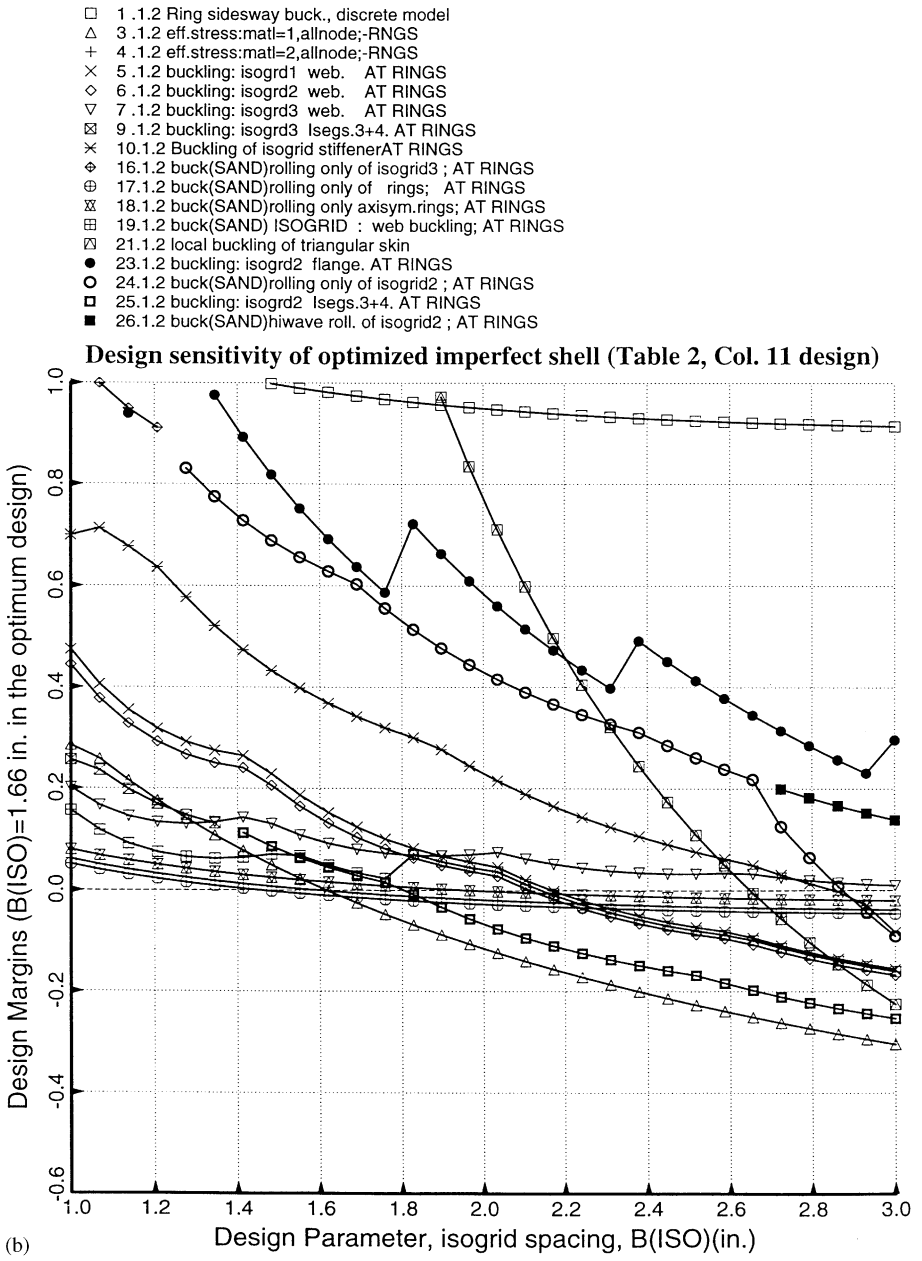

(b)

Fig. 9. (*Continued*).

5. Conclusions

"Global" optimum designs are generated by concatenation of many local optimizations that start from several different designs generated in a random manner. The optimization method is applied to the minimum-weight design of perfect and imperfect internally isogrid and ring stiffened cylindrical shells under uniform external pressure. It is found that for perfect shells it is not especially important

whether or not rings are included but the presence of isogrid stiffening permits significant reduction in optimum weight. The opposite holds for shells with a general buckling modal imperfection of amplitude equal to one per cent of the radius of the shell: for optimum designs the rings are very significant but the isogrid stiffening is not.

References

[1] R.R. Meyer, O.P. Harwood, M.B. Harmon, J.I. Orlando, Isogrid Design Handbook, MDC G4295, McDonnell Douglas Astronautics, Huntington Beach, CA, 1972.

[2] D. Bushnell, PANDA2 — program for minimum weight design of stiffened, composite, locally buckled panels, Comput. Struct. 25 (1987) 469–605.

[3] D. Bushnell, Theoretical basis of the PANDA computer program for preliminary design of stiffened panels under combined in-plane loads, Comput. Struct. 27 (1987) 541–563.

[4] D. Bushnell, Optimization of composite, stiffened, imperfect panels under combined loads for service in the postbuckling regime, Comput. Meth. Appl. Mech. Eng. 103 (1993) 43–114.

[5] D. Bushnell, W.D. Bushnell, Minimum-weight design of a stiffened panel via PANDA2 and evaluation of the optimized panel via STAGS, Comput. Struct. 50 (1994) 569–602.

[6] D. Bushnell, W.D. Bushnell, Approximate method for the optimum design of ring and stringer stiffened cylindrical panels and shells with local, inter-ring, and general buckling modal imperfections, Comput. Struct. 59 (1996) 489–527.

[7] D. Bushnell, Recent enhancements to PANDA2, AIAA Paper 96-1337-CP, Proceedings of the AIAA 37th Structures, Structural Dynamics and Materials Conference, April 1996, pp. 126–182.

[8] D. Bushnell, Optimum design via PANDA2 of composite sandwich panels with honeycomb or foam cores, AIAA Paper 97-1142, Proceedings of the AIAA 38th Structures, Structural Dynamics and Materials Conference, April 1997, pp. 2162–2202.

[9] D. Bushnell, Optimization of panels with riveted Z-shaped stiffeners via PANDA2, in: D. Durban, D. Givoli, J.G. Simmonds (Eds.), Advances in the Mechanics of Plates and Shells, Kluwer Academic Publishers, Dordrecht, 2001, pp. 79–102.

[10] D. Bushnell, Additional buckling solutions in PANDA2, AIAA Paper 99–1233, Proceedings of the AIAA 40th Structures, Structural Dynamics and Materials Conference, April 1999, pp. 302–345.

[11] D. Bushnell, unpublished file called …panda2/doc/panda2.news, which contains a log of all PANDA2 changes since 1987, 2001.

[12] D. Bushnell, BOSOR4: program for stress, buckling, and vibration of complex shells of revolution, in: N. Perrone, W. Pilkey (Eds.), Structural Mechanics Software Series-Vol. 1, University Press of Virginia, Charlottesville, 1977, pp. 11–131.

[13] D. Bushnell, Comput. Struct. 4 (1974) 399–435.

[14] D. Bushnell, AIAA J. 9 (1971) 2004–2013.

[15] D. Bushnell, in: A. Niku-Lari (Ed.), Structural Analysis Systems, Vol. 2, Pergamon Press, Oxford, 1986, pp. 25–54.

[16] D. Bushnell, Comput. Struct. 18 (1984) 471–536.

[17] G.N. Vanderplaats, H. Sugimoto, A general-purpose optimization program for engineering design, Comput. Struct. 24 (1986) 13–21.

[18] W.T. Koiter, The effect of axisymmetric imperfections on the buckling of cylindrical shells under axial compression, Kononkl. Ned. Akad. Wetenschap. Proc. B66 (1963) 265–279.

[19] J. Arbocz, The effect of initial imperfections on shell stability — an updated review, Delft University Faculty of Aerospace Engineering Report LR-695, September, 1992.

[20] J. Arbocz, J.M.A.M. Hol, On the reliability of buckling load predictions, AIAA Paper 94-1371, Proceedings of the 35th AIAA Structures, Structural Dynamics, and Materials Conference, Hilton Head SC, 1993, pp. 514–527.

[21] J. Arbocz, J. Hol, Shell stability analysis in a computer aided engineering (CAE) environment, AIAA Paper 93–133, Proceedings of the 34th AIAA Structures, Structural Dynamics, and Materials Conference, La Jolla, CA, 1993, pp. 300–314.

[22] M. Baruch, J. Singer, Effect of eccentricity of stiffeners on general instability of stiffened cylindrical shells under hydrostatic pressure, J. Mech. Eng. Sci. 5 (1963) 23–27.

[23] J.L. Sanders Jr., Nonlinear theories for thin shells, Q. Appl. Math. 21 (1963) 21–36.

[24] J.L. Sanders Jr., An improved first-approximation theory for thin shells, NASA TR R-24, Langley Research Center, 1959.